Cap-adjacent 2`-*O*-ribose methylation of RNA in *C. elegans* is required for postembryonic growth and germline development in the presence of the decapping exonuclease EOL-1

Eileen Clemens[1], Sarah Brivo[1,6], Mohammed Al-Khafaji[1], Peter Eijlers[1], Maheshika Kurukulasuriya[1], Irmgard U. Haussmann[2], David MacLeod[1,7], Marius Wenzel[3], Berndt Müller[1], Matthias Soller[4,5] and Jonathan Pettitt[1]*

1. School of Medicine, Medical Sciences and Nutrition, Institute of Medical Sciences, University of Aberdeen, Aberdeen, AB25 2ZD, United Kingdom

2. College of Life Science, Birmingham City University, Birmingham, B15 3TN, United Kingdom

3. School of Biological Sciences, University of Aberdeen, Aberdeen AB24 2TX, United Kingdom

4. School of Biosciences, College of Life and Environmental Sciences, University of Birmingham, Edgbaston, Birmingham, B15 2TT, United Kingdom

5. Division of Molecular and Cellular Function, School of Biological Sciences, Faculty of Biology, Medicine and Health, University of Manchester, Manchester, M13 9PT, United Kingdom

6. Current address: Department of Pathology and Immunology, University of Geneva, CMU - Rue Michel-Servet 1, CH-1211 Geneva 4, Switzerland

7. Current address: Wellcome Trust Centre for Cell Biology, Michael Swann Building, Max Born Crescent, Edinburgh EH9 3BF, United Kingdom

* Corresponding author: Tel +44 1224 437516; Email j.pettitt@abdn.ac.uk

ABSTRACT

Cap-adjacent 2`-*O*-ribose methylation (cOMe) of the first two transcribed nucleotides is a conserved feature of RNA polymerase II transcripts in many eukaryotes. In mammals, these modifications are key to a transcript surveillance system that regulates the interferon response, but the broader functions of cOMe remain poorly understood. To understand the role of cOMe in *C. elegans*, we functionally characterised the methyltransferases (CMTR-1 and CMTR-2) responsible for installing these modifications. These enzymes have distinct expression patterns, protein interaction partners and loss of function phenotypes. Loss of CMTR-1 causes dramatic reductions in cOMe, impaired growth and sterility. In contrast, animals lacking CMTR-2 are superficially wild-type phenotype, though CMTR-2 loss enhances the severity of the *cmtr-1* mutant phenotype. Depletion of CMTR-1 causes downregulation of transcripts associated with germline sex determination and upregulation of those involved in the intracellular pathogen response (IPR). We show that absence of the decapping exonuclease, EOL-1, an IPR component, completely suppresses the sterility and growth defects caused of loss of CMTR-1, suggesting that EOL-1 degrades cellular transcripts lacking cOMe. Our work shows the physiological relevance of cOMe in protecting transcripts from decapping exonucleases, raising the possibility that cOMe plays a role in RNA-mediated immune surveillance beyond the vertebrates.

INTRODUCTION

Cap-adjacent 2`-*O*-ribose methylation (cOMe) of RNA was first discovered in mammalian cells several decades ago (Adams and Cory, 1975; Anreiter et al., 2023; Furuichi et al., 1975; Galloway and Cowling, 2019). Subsequent work showed that these modifications are found throughout the Metazoa, as well as in the viruses and protists that infect these organisms. In animals, the first two transcribed nucleotides can harbour cOMe, with methylation of the first transcribed nucleotide being designated "cap1", and methylation of both first and second nucleotides referred to as "cap2". Although these modifications are ubiquitous, their physiological significance remains incompletely understood.

The first defined and the best understood role for cOMe is in preventing activation of an RNA-based immune response (Daffis et al., 2010; Li et al., 2013; Schuberth-Wagner et al., 2015; Züst et al., 2011): an antiviral mechanism consisting of sensor proteins that recognise transcripts lacking cOMe, which brings about the activation of the interferon response. This has created strong selective pressure for viruses to evolve the means to ensure their transcripts are modified by cOMe (Hyde and Diamond, 2015). However, this function does not explain the presence of cOMe in animals that lack the interferon pathway. It also doesn't explain the full significance of cOMe in mammals: loss of either of the two highly conserved methyltransferases, CMTR1 and CMTR2, responsible for cOMe in mice results in embryonic lethality without inducing the interferon pathway (Dohnalkova et al., 2023); and there are multiple lines of evidence supporting diverse roles for cOMe, including the regulation of transcription, RNA splicing, and translation

(Dönmez et al., 2004; Drazkowska et al., 2022; Haussmann et al., 2022; Kuge et al., 1998; Liang et al., 2022; Yu et al., 1998).

Studying cOMe in genetically tractable model organisms such as *Drosophila melanogaster* and *C. elegans* should allow us to understand the functional significance of cOMe from a whole animal perspective. Both organisms have orthologues of mammalian CMTR1 and CMTR2 (Dix et al., 2022; Haussmann et al., 2022). However, detailed functional genetic analysis in *Drosophila* has been hampered by the relatively subtle phenotypic consequences of loss of cOMe. *Drosophila CMTr1/2* double mutants are viable, though they show specific behavioural defects consistent with defects in the spatial regulation of translation in neurons (Haussmann et al., 2022).

Previous studies have shown that subcellular mislocalisation of *C. elegans* CMTR-1can affect the expression of specific genes (Meisel et al., 2024). Here we present a comprehensive analysis of CMTR function, showing that loss of cOMe in *C. elegans* leads to growth retardation and pronounced defects in germline development, with *cmtr-1* loss-of-function mutants conferring a fully penetrant sterile phenotype. Loss of cOMe leads to activation of a set of genes that constitute the intracellular pathogen response (IPR), which are induced by viruses and intracellular pathogens (Lažetić et al., 2023), raising the possibility that as in mammals, there exists a surveillance mechanism to detect transcripts lacking these modifications. From a forward genetic screen for suppressors of *cmtr-1* loss-of-function we identified the decapping exonuclease EOL-1, showing that this enzyme is a major component of the cellular response to transcripts lacking cOMe. Our work suggests evolutionary continuity in the role of cOMe in RNA immune surveillance and provides physiological confirmation of the role of this

89 modification in protecting transcripts from degradation by the DXO/Rai decapping
90 exonuclease family.
91
92 **MATERIALS AND METHODS**
93 **Nematode Strains**
94 *C. elegans* strains were grown using standard culture conditions (Stiernagle, 2006) at
95 20°C unless otherwise indicated. N2 (Bristol) was used as the wild type. The following
96 previously described strains were used in this study: HML1012 (Hills-Muckey et al.,
97 2022); CGC45; CGC66. Strains generated in the current study are described in
98 Supplementary Table 1.

99 The *cmtr-1* deletion allele, *syb3613*, was generated by Fujian Sunybiotech Co. LTD, and
100 obtained as strain PHX3613. The *cmtr-2* deletion allele, *tm4453*, was obtained from the
101 Mitani Lab as strain FX4453. PE1000 was generated from FX4453 by outcrossing six
102 times against N2. Fluorescent-tag/degron knock-in strains were created as described
103 previously (DeMott et al., 2021; Dickinson et al., 2015; Hills-Muckey et al., 2022). The
104 CMTR-1(K244A) mutation was generated through oligonucleotide-templated repair of
105 CRISPR/Cas9 induced double-strand breaks, using the previously described *dpy-10*
106 based co-conversion strategy (Arribere et al., 2014). CRISPR alleles of *eol-1* were made
107 using the same *dpy-10*-based approach, but the injections were performed using
108 PE1176 animals and the resultant F1 progeny grown on 5-Ph-IAA containing plates,
109 selecting for suppression of the sterile phenotype. Alleles were confirmed by Sanger
110 sequencing (Eurofins Genomics). Oligonucleotides used to verify the allelic status of
111 genes, generate guide RNA constructs, and produce homologous repair templates are
112 given in Supplementary Table 1.

113

114 **Transgenic rescuing assay**

115 The wild-type *cmtr-1* cDNA was amplified from total RNA using primers cmcDNAFo and
116 cmcDNARev (Supplementary Table 1). The plasmid backbone, which contains the *rps-0*
117 promoter and *unc-54* 2` -O- UTR, was amplified using primers prpo-u54Fwd and prpo-
118 u54Re (Supplementary Table 1), and the *cmtr-1* cDNA cloned between the *rps-0*
119 promoter and *unc-54* 3` UTR using the NEBuilder HiFi DNA Assembly kit (NEB) to create
120 plasmid pSB2. The plasmid was verified by Sanger Sequencing (Eurofins Genomics).
121 PE1033 worms were co-injected with pSB2 and a plasmid containing *myo-2p::tdTomato*
122 (Eijlers et al., 2024). Transgenic lines were established as previously described (Mello et
123 al., 1991; Nance and Frøkjær-Jensen, 2019). The rescue assay was performed by picking
124 non-tdTomato offspring as L1/L2 larvae to separate plates and scoring their ability to
125 reach fertile adulthood.

126

127 **Fluorescent microscopy**

128 Worms were mounted in 5 µl M9 supplemented with 10 mM sodium azide on 5% agar
129 pads. Images were obtained using either a Zeiss Axioplan 2, equipped with a
130 Hamamatsu Orca ER camera, or a Zeiss Imager M2 upright microscope, equipped with
131 a Hamamatsu Flash 4 LT camera.

132

133 **Western blot**

134 Western blots were performed as described previously (Fasimoye et al., 2022) using
135 lysates from 300 – 500 adult/L4 larvae, or 5000 L1 larvae per well. To detect embryonic

136 expression of CMTR-1/-2 in embryos, 40 µg of total protein from embryonic extracts was
137 loaded per gel lane. For detecting larval expression, GFP-tagged proteins were detected
138 with mouse anti-GFP antibodies (Roche 11814460001), mNeonGreen tagged proteins
139 with rabbit anti-mNeonGreen antibodies (Proteintech, 29523-1-AP) and GAPDH using
140 mouse anti-GAPDH antibodies (Invitrogen AM4300). Secondary antibodies used were
141 anti-mouse or anti-rabbit HRP conjugated IgG antibody (Cell Signalling Technology 7074
142 and 7076). To detect proteins in embryonic extracts, GFP tag Polyclonal antibody
143 (Proteintech, 50430-2-AP) (1:1000 dilution) was used together with the above anti-rabbit
144 secondary (1:3000 dilution). Blots were also stained with amidoblack and quantified
145 using either Fiji (Schindelin et al., 2012)or ImageQuant (Cytiva) software (Fasimoye et
146 al., 2022).

147

148 **Preparation of *C. elegans* embryo extracts**

149 *C. elegans* embryo extracts were prepared essentially as described previously (Eijlers et
150 al., 2024)(see also Supplementary Methods). Extracts were treated with RNase as
151 described previously (Eijlers et al., 2024).

152

153 **Cap-methylation status analysis of mRNA**

154 Total RNA was extracted with Trizol (Sigma) according to the manufacturers description
155 using 20 µg glycogen (Roche) for precipitation. poly(A) mRNA was prepared using the
156 NEBNext® Poly(A) mRNA Magnetic Isolation Module (NEB) by double oligo dT selection
157 according to the manufacturer's instructions.

158 For the analysis of 5` cap structures, 5 µg total RNA was used for decapping by yDcpS in
159 20 µl for 1 h at 37°C according to the manufacturer's instruction (NEB). The RNA was
160 extracted by phenol/$CHCl_3$ and ethanol precipitated in the presence of glycogen. The
161 RNA was then labeled in a total volume of 20 µl containing 2 µl capping buffer (NEB), 1 µl
162 SAM (2 mM), 0.25 µl ^{32}P-αGTP (3000 Ci/mmol, 6.6 µM; Hartmann Analytics), 0.5 µl RNase
163 Protector (Roche) and 0.5 µl capping enzyme (NEB) by incubation for 1 h at 37°C. The
164 volume was then increased to 50 µl with water and poly(A) RNA selected as described
165 above. The RNA was then digested on the beads in 5 µl using 0.5 µl NEB buffer 3 and 0.5
166 µl RNase I for 2 h, and then 10 µl gel loading buffer was added (98% deionized
167 formamide,10 mM EDTA, 0.025% xylene cyanol FF and 0.025% bromphenol blue);
168 products were analysed on 22% denaturing polyacrylamide gels (National Diagnostics)
169 and pre-run for 2 h. Gels were soaked in 20% PEG400, 10% acetic acid and 40% methanol
170 for 10 min and then dried on a Whatman 3MM paper. Dried gels were then exposed to a
171 storage phosphor screen (Bio-Rad) and scanned by a Molecular Imager FX in
172 combination with QuantityOne software (Bio-Rad). Markers were prepared as described
173 previously (Dix et al., 2022; Haussmann et al., 2022).

174 For the analysis of the first nucleotide in mRNA, 5 µg poly(A) mRNA was purified as
175 described above and 5 µl incubated with terminator nuclease (Epicenter), according to
176 the manufacturer's instructions, to remove rRNA followed by phenol/$CHCl_3$ and ethanol
177 precipitation in the presence of glycogen (Roche). The mRNA was then decapped using
178 RppH (NEB) and dephosphorylated by Antarctic phosphatase (NEB) in NEB buffer 2
179 supplemented with 0.1 mM $ZnCl_2$ in 20 µl. Then the RNA was extracted by phenol/$CHCl_3$
180 and precipitated in the presence of glycogen. The 5`-ends of dephosphorylated mRNAs
181 were then labelled using 10 units of T4 PNK (NEB) and 0.25 µl ^{32}P-γATP (6000 Ci/mmol,

182 12.5 µM; Hartmann Analytics). The labelled RNA was precipitated, and resuspended in
183 10 µl of 50 mM sodium acetate buffer (pH 5.5) and digested with nuclease P1 (SIGMA) for
184 2 h at 37°C. Two microliters of each sample was loaded on cellulose F TLC plates (20× 20
185 cm; Merck) and run in a solvent system of isobutyric acid:0.5 M NH_4OH (5:3, v/v, solvent
186 A), as first dimension, and isopropanol:HCl:water (70:15:15, v/v/v, solvent B) or sodium
187 phosphate, 0.1 M (pH 6.8), ammonium sulfate, n-propanol (100:60:2, v/w/v, solvent C),
188 as the second dimension. TLCs were repeated from biological replicates. The identity of
189 the nucleotide spots was determined as described (Keith, 1995; Kruse et al., 2011). TLCs
190 were exposed to a storage phosphorscreen (Bio-Rad) and scanned by a Molecular Imager
191 FX in combination with QuantityOne software (Bio-Rad).

192

193 **Monitoring SL1 *trans*-splicing using quantitative PCR**

194 RNA was isolated from embryonic extracts prepared from PE1176 and PE1220 embryos,
195 treated for 4 h with either 50 µM 5-Ph-IAA-AM in DMSO, or control treated in DMSO by
196 extraction with TriZol, and then purified using the PureLink RNA Mini kit (Life
197 Technologies), with modifications for TRIzol treated samples and DNase treatment, as
198 described by the manufacturer. Reverse transcription and analysis by qPCR were done
199 as described (Eijlers et al, 2024, Philippe et al, 2017). Analyses were done as three
200 technical replicates. Shown are ΔC_T values derived for each replicate (Schmittgen and
201 Livak, 2008).

202

203 ***In vitro* spliced leader *trans*-splicing assays.**

204 For extract preparation, PE1176 and PE1220 animals were grown in liquid culture and
205 embryos were isolated and treated with 50 µM 5-PH-IAA-AM or control-treated with
206 DMSO as described (Eijlers et al., 2024), except that treatment was for 4h. Extracts
207 were then prepared as described (Eijlers et al., 2024) and stored at -80°C. The synthetic
208 SL *trans*-splicing substrate, consisting of *rps-3* genomic DNA containing 404 bp of 5`
209 UTR sequence (including 382 bp of outron sequence upstream of the known SL1 *trans*-
210 splice site) and extending 266 base pairs downstream from the ATG translation start
211 site, was amplified from *C. elegans* genomic DNA using primers *rps-3*genFwd and *rps-*
212 *3*genRev (Supplementary Table 1). The resulting amplicon was inserted into pBlueScript
213 KS(-) cleaved with XbaI using NEB HIFI gene assembly to produce pBS-*rps-3*. The
214 sequence was confirmed by Sanger sequencing (Eurofins Genomics). pBS-*rps-3* DNA
215 linearised with EcoRI was transcribed with T7 RNA polymerase using the MEGAscript®
216 kit (Invitrogen). This produces a synthetic *rps-3* RNA with a 3`-end derived from
217 pBlueScript KS(-) that serves as a primer binding site in PCR. RNA was extracted using
218 phenol/chloroform, concentrated by ethanol precipitation, resuspended in RNase-free
219 water and purified using MicroSpin G-25 columns (Cytiva). RNA concentration was
220 determined by measuring absorption at 260 nm assuming 1 AU = 40 µg/ml.

221 *In vitro* SL1 *trans*-splicing reactions were done essentially as described (Lasda et al.,
222 2011). 15 µl reactions were done in 10 mM Tris-HCl (pH 8.0), 60 mM KCl, 4 mM $MgCl_2$, 2
223 mM ATP, 20 mM creatine phosphate, 50 µg/ml creatine kinase, 2 mM DTT, 3 % PEG 8000,
224 0.25 mM EDTA, 5% glycerol, 0.5 mM PMSF, 2 U/µl RNaseOUT, 8 µg/µl embryonic extract
225 and 2.5 ng/µl synthetic *rps-3* mRNA. Control reactions were performed without addition
226 of ATP, creatine phosphate and creatine kinase. Incubation was at 15°C for 2 h.

227 For analysis by one-step RT-PCR, reactions were diluted 1:80 in RNase-free MilliQ water
228 and aliquots were then used for one-step RT-PCR using the Luna® Universal One-Step
229 RT-qPCR kit (NEB) according to the manufacturer's instructions; primers are given in
230 Supplementary Table 1. Reactions were done with 1 µl or 2 µl diluted reactions and
231 analysed by agarose gel electrophoresis, or quantified using a LightCycler 480 (Roche),
232 with software release 1.5.1.62 Sp3. qPCR data was analysed using the ΔC_T method
233 (Schmittgen and Livak, 2008). Products P1, P2 and P3 were identified by cloning into
234 pGEM-T Easy (Promega) followed by Sanger sequencing (Eurofins Genomics).

235

236 **Protein Immunoprecipitation**

237 Immunoprecipitations of GFP-tagged proteins were performed in triplicates or
238 quadruplicates using anti-GFP nanobody coupled agarose beads and control agarose
239 beads (GFP-Trap and control agarose beads, Chromotek GmbH), essentially as
240 described previously (Eijlers et al., 2024).

241

242 **Protein analysis by LC-MS/MS and differential protein expression analysis**

243 Proteomic analysis by mass spectrometry was done at the Aberdeen Proteomics unit as
244 previously described (Eijlers et al., 2024; Fasimoye et al., 2022). MaxQuant version
245 1.6.5.0 (Cox and Mann, 2008) was used to process the raw data files with the *C. elegans*
246 reference proteome UP000001940 downloaded on the 24th of August 2021 as described
247 (Eijlers et al., 2024), except that the feature "match between runs" was applied. The
248 MaxQuant protein group files were further analysed using Perseus version 1.6.5.0 as
249 described (Eijlers et al., 2024). Graphs were drawn in GraphPad Prism.

250

251 **RNA extraction and mRNA-Seq**

252 Prior to RNA extraction, the worms were treated with 5-Ph-IAA when they reached the L3
253 larval stage. Therefore, synchronised PE1176 L1s were grown in liquid culture for 22.5 h
254 until they started moulting into larval stage 3. They were then divided into two and
255 plated on control plates or 5-Ph-IAA plates, respectively, and cultured for 16 h, at which
256 point the animals had started moulting into the L4 larval stage. Worms were washed off
257 NGM plates using M9 and washed 3 times by centrifugation at 749g for 2 min at 4°C.
258 Subsequently, 1 ml of Trizol (TRI Reagent, T9424, Sigma Aldrich) was added per 50 µl of
259 worm pellet and samples frozen in liquid nitrogen. Samples were thawed at 37°C and
260 re-frozen four times. They were then vortexed for 30 s, left to rest for 30 s and the
261 vortex/rest process repeated for a further three times. Phase separation by addition of
262 chloroform and recovery of RNA was done as described by the manufacturer. The
263 aqueous fraction was transferred to a low DNA-binding-tube and diluted 1:1 with 70%
264 ethanol. RNA was purified using PureLink RNA Mini Kit (Thermo Fisher Scientific), using
265 the on-column DNase-treatment option. Three libraries per treatment group were
266 sequenced on an Illumina NovaSeq instrument, generating 2x150bp paired-end reads
267 (Novogene UK Ltd).

268

269 **Differential gene expression analysis**

270 The quality of the raw reads was inspected in FASTQC 0.11.9 (Andrews, 2010) and
271 MULTIQC 1.12 (Ewels et al., 2016), and bases with a Phred score below 20 were
272 trimmed using TRIMGALORE 0.6.6 (Krueger, 2015). The trimmed reads were then aligned

273 to the *C. elegans* WB235 reference genome using HISAT2 2.2.0 (Kim et al., 2015).
274 Alignments were processed using SAMTOOLS 1.14 (Li et al., 2009). Gene-level read
275 counts were obtained using FEATURECOUNTS 2.0.2 (Liao et al., 2014), quantifying
276 against exon annotations and assigning fractional counts to all alignment locations of
277 multi-mapping reads.

278 The read counts were analysed in DESeq2 1.42. (Love et al., 2014), identifying
279 differentially expressed genes with an FDR (Benjamini and Hochberg, 1995) significance
280 threshold of 0.05, and shrinking fold changes at low-count genes using the *apeglm*
281 method (Zhu et al., 2019). Significantly differentially expressed genes (DEGs) were
282 examined for overrepresentation GeneOntology terms (biological process ontology)
283 using CLUSTERPROFILER 4.10.0 (Yu et al., 2012) with the *org.Ce.eg.db* 3.18.0 database
284 (June 2024). The GO results were simplified by removing terms at graph levels 1-3,
285 clustering GO terms semantically with the Wang method at a similarity cutoff of 0.7 (Yu
286 et al., 2010), and retaining for each cluster the single GO term with the smallest *P*-value.

287

288 **Data analysis using RStudio**

289 RStudio was used for data analysis and graph generation (http://www.rstudio.com/).
290 The following R packages were used: ggplot2 (Wickham, 2016), dplyr
291 (https://dplyr.tidyverse.org/), carData/car (10.32614/CRAN.package.car), multcomp
292 (10.32614/CRAN.package.multcomp), ggpubr (https://rpkgs.datanovia.com/ggpubr/),
293 rstatix (https://rpkgs.datanovia.com/rstatix/), tibble (https://tibble.tidyverse.org/),
294 RcolorBrewer (10.32614/CRAN.package.RColorBrewer).

295

296 **Screen for suppressors of *cmtr-1* loss-of-function**

297 PE1176 worms were subjected to a standard ethyl methylsulfonate (EMS) mutagenesis.
298 Thirty F1 cultures were established by subjecting the mutagenised parental animals to
299 alkaline hypochlorite treatment and plating 500 F1 animals per 9 cm plate. The
300 mutagenised animals and their F1 progeny were propagated on standard NGM agar
301 plates. The F2 embryos from alkaline hypochlorite treated F1s were plated onto 9 cm
302 NGM plates supplemented with 1 μM 5-Ph-IAA. Suppressor mutants, identified on the
303 basis of presence of eggs in the uterus of adult F2s, were picked to establish lines,
304 taking care to only maintain one line for each F1 lineage.

305

306 **Genetic analysis of suppressor mutants**

307 We reasoned that our screen would generate two classes of fertile mutants: those that
308 are *bona fide* extragenic suppressors of mNG^AID::CMTR-1 knockdown; and loss-of-
309 function mutants in the *TIR1* transgene, which would lead to 5-Ph-IAA-independent
310 expression of mNG^AID::CMTR-1. We thus screened each suppressor line for the
311 presence of nuclear mNeonGreen fluorescence when grown on media containing 5-Ph-
312 IAA. Mutant lines that showed mNeonGreen fluorescence in the presence 5-Ph-IAA
313 were assumed to be *TIR1* mutants; the *TIR1* coding region for a subset of these was
314 sequenced to confirm this assumption. Amplicons generated from single-worm PCRs
315 using primer pairs TIR1Fwd+TIR1Rev1 and TIR1fo1+TIR1re2 were sequenced using the
316 same oligos to prime Sanger sequencing reactions (Eurofins Genomics).

317 Mutants that lacked nuclear mNeonGreen fluorescence in the presence of 5-Ph-IAA
318 were assumed to be genuine epistatic suppressors and were backcrossed with non-
319 mutagenised PE1176. The resultant strains were crossed into the *cmtr-1(syb3613)*
320 background to determine the ability of the suppressor mutations to suppress the sterile
321 phenotype of the *cmtr-1* null allele.
322

323 **Sib-Selection and DNA Preparation**

324 Two suppressor strains, PE1237 (*fe152*) and PE1245 (*fe154*), were subject to a sibling
325 subtraction/whole genome sequencing method adapted from a previously reported
326 method (Joseph et al., 2017). Male PE1053 worms were crossed with hermaphrodites
327 from PE1237/1245. F1 progeny carrying the *feEx342* transgenic array were identified on
328 the basis of pharyngeal tdTomato expression, picked to separate plates, and allowed to
329 segregate F2 progeny. Two hundred *feEx342* transgenic F2s were picked singly to
330 separate 35 mm plates and allowed to propagate. Homozygous suppressor lines (Sup)
331 were identified on the basis of the presence of fertile non-tdTomato F3/F4 worms, and
332 the absence of non-tdTomato "scrawny" F3/F4 worms, the latter being observed on
333 plates whose frequency suggested that these were broods of suppressor heterozygotes.
334 Lines that failed to inherit suppressor mutations (Nonsup) were identified on the basis
335 of the complete absence of fertile non-tdTomato F3/F4 worms. Contaminated plates
336 were discarded. Worms were washed off plates, and Sup/Nonsup cultures pooled as
337 outlined previously (Doitsidou et al., 2010). The number of 35 mm F2 plates used to
338 generate the Sup and Nonsup pools were as follows: *fe152* Sup = 16; *fe152* Nonsup =
339 19; *fe154* Sup = 19; *fe154* Nonsup = 19. Genomic DNA was prepared using the Qiagen
340 Puregene Tissue Kit (Qiagen, 158063) as described previously (Doitsidou et al., 2010).

One library per pool was sequenced on an Illumina NovaSeq X Plus instrument, generating 2x150bp paired-end reads (Novogene UK Ltd).

Variant Detection

Quality control of the raw reads was carried out using FASTQC 0.11.9 (Andrews, 2010) and MULTIQC 1.12 (Ewels et al., 2016). Adaptor removal and trimming of bases with a Phred score below 20 was performed using TRIMGALORE 0.6.6 (Krueger, 2015). The trimmed reads were then aligned to the *C. elegans* WB235 reference genome using BWA MEM 0.17.17 (Li and Durbin, 2010). Variant detection was done for all libraries together in a single run of FREEBAYES 1.3.6 (Garrison and Marth, 2012), and the resultant VCF files were filtered and manipulated using BCFTOOLS 1.14 (Danecek et al., 2021). We considered biallelic SNPs with experiment-wide genotyping quality of at least 20 and at least 10 reads in each library, and retained SNPs fixed for the alternative allele (>90% of read depth) in Sup libraries and fixed for the reference allele (>90% of read depth) in Nonsup libraries. SNPEFF 4.3t (Cingolani et al., 2012) was then used to functionally annotate the candidate SNPs identified by this filtering strategy.

RESULTS

CMTR-1 is required for oocyte cell fate

To determine the role of cOMe in *C. elegans,* we studied the phenotypes of animals lacking one or both CMTR proteins. We obtained a deletion allele, *syb3613*, of *cmtr-1* (SunyBiotech), which removes the methyltransferase domain, and is thus a predicted null allele. We also studied a deletion allele of *cmtr-2*, *tm4453*, that deletes key residues in the methyltransferase domain (Dix et al., 2022). While *cmtr-1(syb3613)* homozygotes were able to reach adulthood, they were 100% sterile (Figure 1A,B) and were thinner than similarly staged *syb3613* heterozygotes.

We found that the sterility was due to defects in the formation of oocytes, which ranged from a completely masculinised germline that produced only sperm, through to animals that were able to produce only a few embryos that failed to develop (Figure 1D,E,H). In all cases, *cmtr-1(syb3613)* homozygotes showed much smaller germlines than wild-type worms, something also observed in mutants that cause masculinised hermaphrodite germlines (Kimble and Crittenden, 2007).

We confirmed that the defects observed were due to loss of *cmtr-1* function by demonstrating that an extrachromosomal transgene consisting of the *cmtr-1* cDNA expressed under the control of the *rps-0* promoter rescued the germline sterility defects (Figure 1F,G). As part of this analysis we found that offspring that failed to inherit the extrachromosomal transgene generally showed a more severe phenotype than the offspring of heterozygous mothers, displaying more severe growth defects (Figure 1G). Since extrachromosomal transgenes are generally silenced in the germline (Kelly et al., 1997), this likely indicates that there is a significant *cmtr-1* maternal contribution, which

380 is absent from the non-transgenic offspring of transgenic mothers. The more severe
381 phenotypes of these animals indicates that the loss of *cmtr-1* function impacts other
382 tissues beyond the germline.

383 In contrast to loss of *cmtr-1*, *cmtr-2* loss-of-function homozygotes are superficially wild
384 type (Dix et al., 2022). To investigate whether loss of *cmtr-2* function influenced the
385 *cmtr-1* loss-of-function phenotype, we examined the phenotype of *cmtr-1*; *cmtr-2*
386 double mutants. This analysis showed that loss of *cmtr-2* enhanced the phenotype of
387 *cmtr-1* single mutants (Figure 1H). Thus, CMTR-2 contributes to the role played by
388 CMTR-1.

389 The failure of oocyte differentiation in *cmtr-1* mutant homozygotes suggested that
390 CMTR-1 function is required for some component(s) of the sperm-oocyte switch. To
391 determine when CMTR-1 protein is required during larval development for oocyte cell
392 fate, we generated an auxin-inducible degeneration (AID) allele of *cmtr-1*, which
393 expresses endogenous CMTR-1 tagged with the auxin-inducible degron (AID) peptide
394 and monomeric NeonGreen (mNG^AID::CMTr1). This strain (PE1176) also expresses the
395 *A. thaliana* TIR1(F79G) transgene necessary for auxin-dependent protein depletion
396 (Hills-Muckey et al., 2022). Growing this strain in the presence of 5-Ph-IAA showed rapid
397 depletion of mNG^AID::CMTr1 (Supplementary Figure 1), and such worms were 100%
398 sterile and showed reduced body size compared to untreated controls (Figure I).

399 Using this strain, we performed a series of experiments designed to deplete
400 mNG^AID::CMTR-1 at specific times during postembryonic development. We initiated
401 synchronous cultures of 50 starved, first-stage larvae (L1s) on control plates and
402 transferred them to 5-Ph-IAA plates at defined times (Figure 1J). We also performed the

403 inverse experiment, culturing L1s on 5-Ph-IAA plates and transferring them to control
404 plates at the same time points. This “auxin-shift” experiment (named by analogy to
405 temperature-shift experiments performed with temperature-sensitive mutants)
406 revealed that 5-Ph-IAA depletion of mNG^AID::CMTR-1 resulted in sterility only during a
407 critical time period between approximately 24 and 40 hours following initiation of
408 starved L1 larval development. The critical period during which CMTR-1, and thus
409 cOMe, is required corresponds roughly to the L3 and L4 larval stages. Given that the
410 sperm-oocyte switch occurs during the L4 stage (Kimble and Crittenden, 2007), the
411 time-window during which CMTR-1 is required suggest that this is when transcripts
412 involved in germline sex determination need to be modified by cOMe for normal
413 germline cell fate.

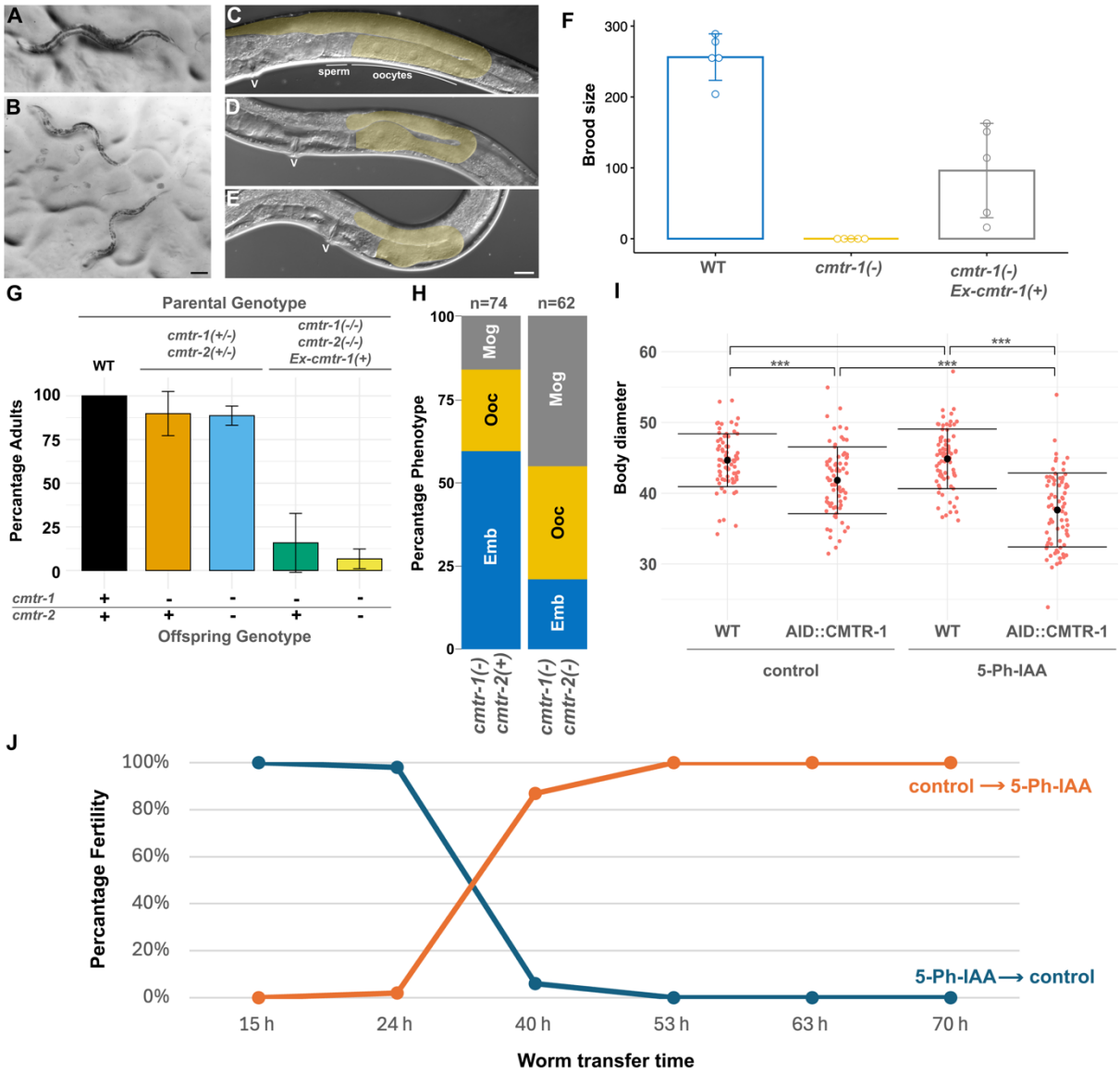

Figure 1. Loss of *cmtr-1* function results in defects in germline development and body size. Representative *cmtr-1(syb3613)/+* heterozygote (A), compared to sibling *cmtr-1(syb3613)* homozygotes (B). Wild type young adult hermaphrodite (C), showing posterior gonad arm (gold overlay), compared to the same regions of *cmtr-1(syb3613)* homozygotes, one of which shows a single defective oocyte (D), and the other has a fully masculinised germline that has only produced sperm (E). Position of the vulva is indicated by "v". Scale bars represent 100 µm (A,B) and 20 µm (C,D,E). (F) Transgenic expression of *cmtr-1* cDNA under the control of the *rps-0* promoter (*Ex-cmtr-1(+)*) rescues the fertility defects of *cmtr-1(syb3613)* mutants (*cmtr-1(-)*). (G) Comparison of the number of worms reaching adulthood 72 hours after hatching (n > 61 for each experiment). Mutant offspring (*cmtr-1(-)*; *cmtr-2(+)* or *cmtr-1(-)*; *cmtr-2(+)*) of transgenic parents (transgene is indicated '*Ex-cmtr-1(+)*)are slower-growing compared to

genetically identical offspring of heterozygous parents. (H) Loss of *cmtr-2* increases the severity of the *cmtr-1* loss-of-function germline defects. Histograms show the distribution of the three germline defect classifications caused by loss of *cmtr-1* function: production of a few arrested embryos (Emb, blue); abortive oocyte production (Ooc, gold); masculinised germline (Mog, grey). (I) Worm diameter, measured at the mid-body, for worms homozygous for the mNG^AID::*cmtr-1* allele subject to control and 5-Ph-IAA treatment. Two-way ANOVA and a Tukey post hoc test were used to determine p-values; * < 0.05, ** < 0.01, *** < 0.001, n = 75 animals per group. (J) “Auxin-shift” experiment to determine when CMTR-1 function is required for fertility. Starved L1 larvae (n=50) were placed on either 5-Ph-IAA or control plates for the indicated time period, before being transferred to the alternative plate type (i.e. those on 5-Ph-IAA plates were moved to control plates, and vice versa). The worms were then left on the second plate, allowed to reach adulthood, and scored for fertility.

440 **The *C. elegans* CMTR proteins show distinct expression patterns and protein-**
441 **protein interactions**

442 Studies in cultured mammalian cells and *Drosophila* indicated that the two CMTR
443 proteins have conserved, distinct subcellular distributions: in both cases, CMTR1 is
444 primarily nuclear, whereas CMTR2 is both nuclear and cytoplasmic (Haline-Vaz et al.,
445 2008; Haussmann et al., 2022; Werner et al., 2011). Using strains that express GFP-
446 tagged alleles of the endogenous proteins, we found that *C. elegans* CMTR proteins are
447 nuclear throughout postembryonic development (Figure 2A-D), being expressed in
448 most, if not all cells, though CMTR-2 does not appear to be as strongly expressed in the
449 nucleus as CMTR-1. While the overall levels of the two proteins are similar in embryos,
450 as judged by Western blot (Figure 2H), the intracellular localisation of the two proteins is
451 strikingly distinct: CMTR-1 is predominantly nuclear (Figure 2E), in contrast to CMTR-2,
452 which is strongly cytoplasmic (Figure 2F, compare to Figure 2G).

453 To investigate the functional significance of the distinct localisation of the proteins
454 during embryogenesis further, we performed immunoprecipitation analyses from
455 embryonic lysates to assess their respective protein-protein interactions. This analysis
456 revealed that the two proteins have non-overlapping protein partners: CMTR-1 showed a
457 rich set of protein-protein interactions (Figure 3A-C); while CMTR-2 displayed a paucity
458 of interactors (Figure 3D, E); none of them matching those we found for CMTR-1. The
459 lack of overlap in protein interaction partners is consistent with the low levels of CMTR-
460 2 in the nucleus (Figure 2E,F) in embryos, but this analysis fails to shed light on the
461 functional significance of the cytoplasmic enrichment of CMTR-2.

462 *C. elegans* CMTR-1 showed broadly the same protein-protein interactions with a suite of
463 pre-mRNA processing factors that were observed for mammalian cells (Simabuco et al.,
464 2019), with components of the spliceosome, heterogeneous nuclear ribonucleo-
465 proteins and ribosomal proteins being prominent interaction partners (Figure 3A-C). We
466 also saw an interaction with SNA-3, a component of the spliced leader *trans*-splicing
467 machinery (Fasimoye et al., 2022) that has previously been shown to associate with
468 nascent RNA polymerase II transcripts (Eijlers et al., 2024). Many of the interactions
469 were abolished by RNase treatment, consistent with CMTR-1 interacting with them by
470 virtue of binding to the same transcript. However, there are notable interactions that
471 were preserved in RNase treated samples, included the previously well-defined CMTr1
472 interacting protein, DHX15 (DDX-15 in *C. elegans*)(Inesta-Vaquera et al., 2018;
473 Toczydlowska-Socha et al., 2018), and some core components of the spliceosomal
474 catalytic complex.

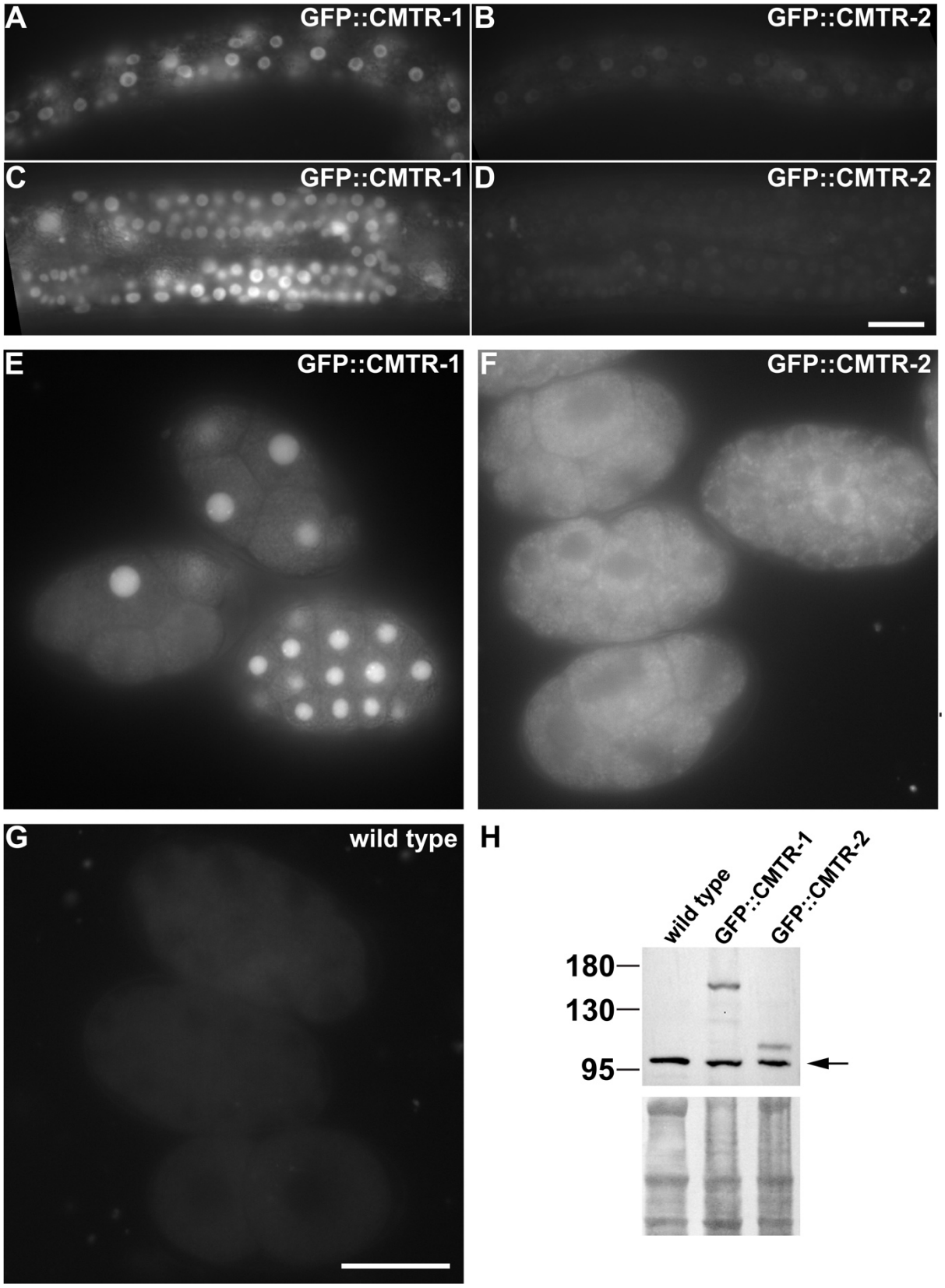

Figure 2. CMTR-1 is constitutively nuclear but CMTR-2 subcellular localisation is developmentally regulated. Representative images showing the respective expression

of GFP tagged CMTR-1 (A, C, E) or CMTR-2 (B, D, F) in L2 larval stage epidermis (A, B), L4 germlines (C, D) and early embryos (E, F). Wild type embryos (G) show the level of embryonic background autofluorescence. Images in A – D and E - G were taken at the same camera exposure settings. Scale bars indicate 20 μm. (H) Western blot of GFP-tagged CMTR-1 and CMTR-2 in embryonic extracts probed with anti-GFP polyclonal antibody. Specific signals are absent from wild type embryos. Arrow indicates non-specific primary anti-GFP antibody immunoreactivity. Amido black stained immunoblot indicates loading of protein in each lane.

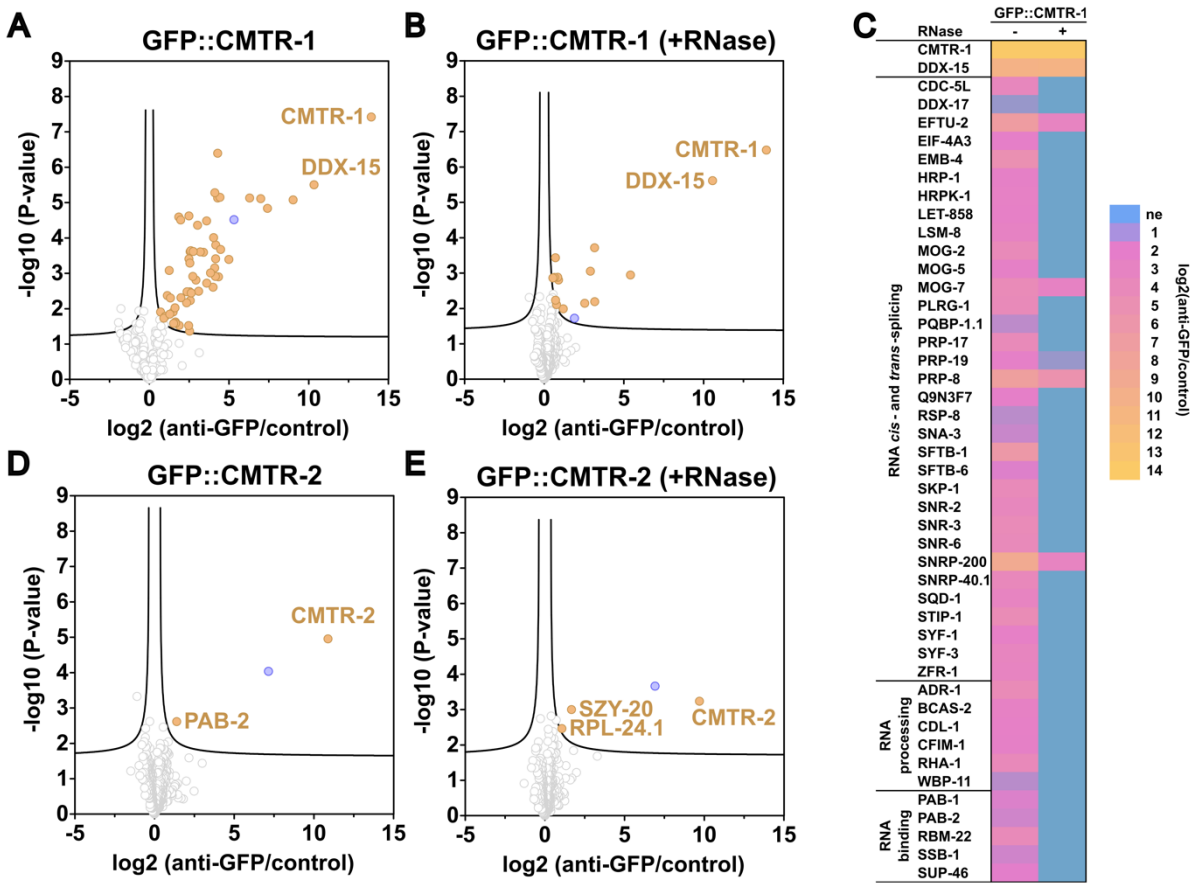

Figure 3. CMTR-1 and CMTR-2 show distinct protein-protein interaction partners

Proteins enriched by co-immunoprecipitation with GFP::CMTR-1 (A, B, C) and GFP::CMTR-2 (D, E) from PE1001 and PE991 embryonic extracts treated without (A, D) and with RNase (B, E). Immunoprecipitations were performed in triplicate or quadruplicate using anti-GFP nanobodies coupled to agarose beads, or control agarose beads. Immunoprecipitated proteins were identified by label-free quantification as described (Eijlers et al 2024). Graphs show enrichment in anti-GFP nanobody immunoprecipitations (anti-GFP) compared to bead only controls (control) and the false discovery rate (y-axis). Proteins that were significantly enriched are shown in gold. The significance cutoff curve is drawn in black (false discovery rate <=0.05 and S0 of 0.1). TBH-1 (blue), a dopamine β-hydroxylase, is found in all immunoprecipitations but our previous work suggests that it non-specifically associates with GFP-tagged proteins (Eijlers et al., 2024; Fasimoye et al., 2022). (**C**) Heatmap summarising the enrichment of spliceosome components, RNA processing factors and RNA binding proteins in immunoprecipitation of GFP::CMTR-1. Proteins were grouped using the gene ontology annotation retrieved from UniprotKB (Ashburner et al., 2000; Gene Ontology

Consortium et al., 2023; The UniProt Consortium et al., 2023). ne: not enriched. For complete lists of identified proteins see Supplementary Table 2.

505 **Loss of cOMe is the cause of the *cmtr-1* loss-of-function phenotype**

506 The phenotypic impact of loss of *cmtr-1* compared to *cmtr-2* suggested that CMTR-1
507 function might be more important for cOMe modification of transcripts than CMTR-2.
508 This was supported by our previous analysis, which showed that loss of *cmtr-2* did not
509 detectably affect cOMe levels (Dix et al., 2022). To investigate the dependence of cOMe
510 on CMTR-1, we assayed RNA derived from animals in which mNG^AID::CMTR-1 was
511 knocked down on its own, and in combination with the *cmtr-2(tm4453)* loss-of-function
512 mutation. Using a sensitive assay based on recapping mRNA with ^{32}P-alpha-GTP,
513 followed by RNase I digestion to detect cOMe in small amounts of mRNA (Anreiter et al.,
514 2020; Dix et al., 2022; Haussmann et al., 2022), we found that cOMe modified RNA
515 (cap1) was almost completely abolished (Figure 4A). Note that using this assay, we were
516 not able to detect cap2 modifications, consistent with a previous study that this cap2 is
517 largely absent from *C. elegans* (Despic and Jaffrey, 2023). This assay also revealed that
518 CMTR-2 makes a negligible impact on cap1 levels, as we previously demonstrated (Dix
519 et al., 2022). Thus, CMTR-1 is the important determinant of cOMe in *C. elegans*,
520 consistent with its strong loss-of-function phenotype.

521 We then looked specifically at cap1 in poly(A) mRNA derived from animals lacking
522 functional CMTR-2 and depleted of mNG^AID::CMTR-1 by treatment with 5-Ph-IAA to
523 find that cOMe is essentially absent (Figure 4B-G). Of note, the first transcribed
524 nucleotide for the majority of *C. elegans* mRNAs will be the guanosine originating from
525 the *trans*-spliced leaders. As shown by separation of the second dimension in solvent
526 C, the spliced leader is also 2`-*O*-ribose methylated by CMTR-1 (Figure 4E-G), as
527 expected for an RNA polymerase II transcript.

Previous studies in mammals have shown that around 50% of CMTR1 is in a complex with DHX15, and that this interaction represses its methyltransferase activity (Inesta-Vaquera et al., 2018; Toczydlowska-Socha et al., 2018). CMTR1 also influences RNA polymerase II recruitment to transcription start sites and the transcription of histone and ribosomal protein genes (Liang et al., 2022). We thus wanted to confirm that the *cmtr-1* loss-of-function phenotype was due solely to loss of cOMe; in other words that it was dependent on CMTR-1 methyltransferase activity.

To address this, we engineered a missense mutation, K244A, into the endogenous *cmtr-1* gene. The orthologous mutation in human CMTR1 (K239A) has previously been show to abolish methyltransferase function (Bélanger et al., 2010; Feder et al., 2003), and the lack of function of this mutation in *C. elegans* has been assessed in transgene rescue experiments (Meisel et al., 2024). We carried out site-directed mutagenesis of the *cmtr-1* allele that expresses CMTR-1 with a N-terminal GFP tag (Figure 2), allowing us to monitor the impact of the K244A mutation on the expression and localisation of CMTR-1 (Figure 4H,I). All worms homozygous for the K244A (*fe175*) allele showed the same recessive sterile and growth defective phenotypes displayed by the *syb3613* mutation, and these phenotypes were complemented by the *rps-0::cmtr-1(+)* transgene (Figure 4J). Since these worms specifically lack the methyltransferase activity of CMTR-1, this indicates that loss of cOMe is the cause of the germline phenotypes.

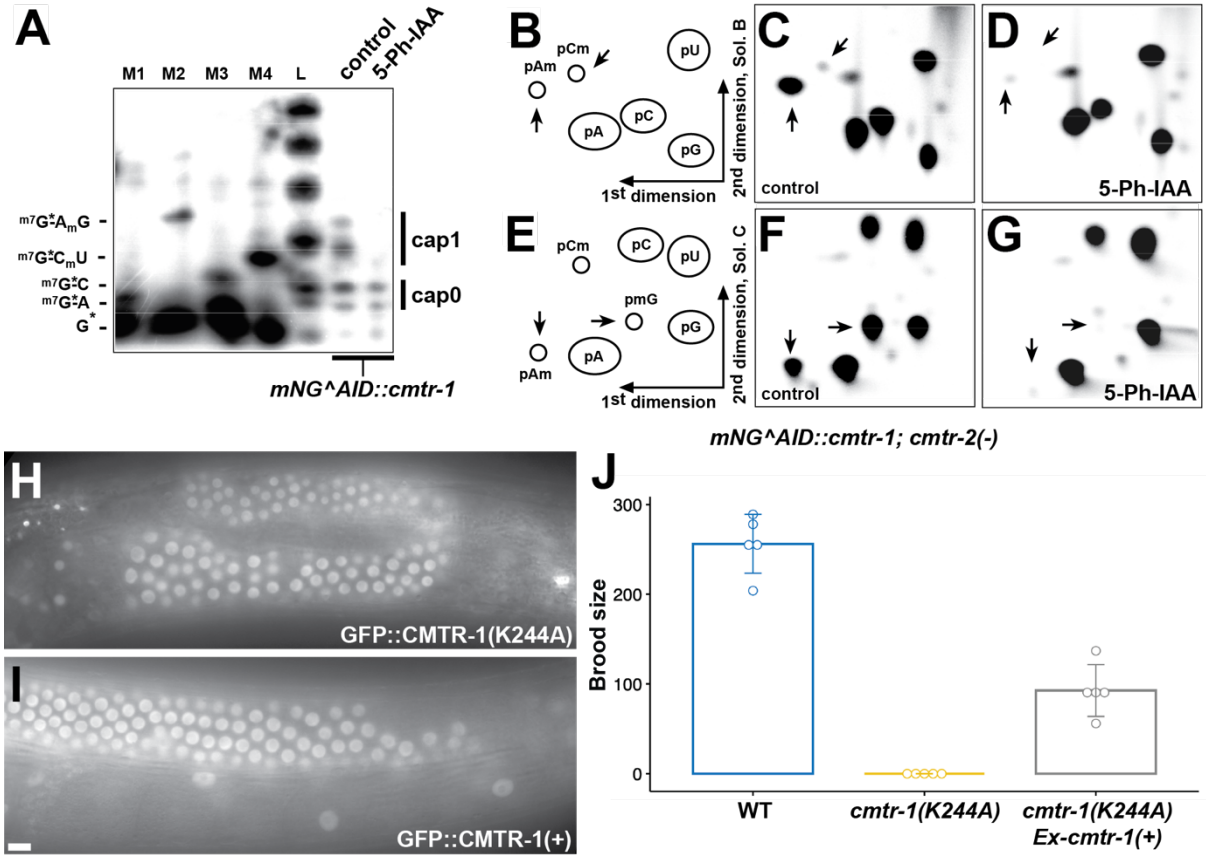

**Figure 4. CMTR-1 is required for cap-adjacent 2`-O-ribose methylation in *C. elegans*.** Analysis of cap-adjacent 2`-*O*-ribose RNA methylation with (control) and without (5-Ph-IAA) mNG^AID::CMTR-1. (A) Recapping assay to detect mRNA using ^{32}P-αGTP. 5' cap structures were separated on a 22% denaturing polyacrylamide gels after digestion with RNase I (lanes 6-7, right). Markers (M1-4) are RNase I digested ^{32}P-αGTP capped oligonucleotides. 2`-*O*-ribose methylation (N_m) was added using vaccinia CMTr. Sequences of markers are shown on the left. (B - G) Two dimensional thin-layer chromatograms (2D-TLCs) showing modifications of the first cap-adjacent nucleotides prepared from total RNA isolated from worms homozygous for the mNG^AID::*cmtr-1* and *cmtr-2(-)* alleles, grown on control (C, F) or 5-Ph-IAA plates (D, G). (B, E) Schematic diagrams of a 2D-TLC, depicting the positions of unmodified and 2`-*O*-ribose

methylated nucleotides. One set of chromatograms (C, D) was run in solvent B for the second dimension, another set (F, G) was run in solvent C. 2`-O-ribose methylated nucleotides are indicated by arrows. (H) Representative germline GFP fluorescence of an animal expressing GFP-tagged CMTR-1(K244A), compared to GFP-tagged wild-type CMTR-1 protein. (J) Brood counts of wild-type (data from Figure 1F) and animals homozygous for the K244A mutation, in the absence and presence of the wild-type *cmtr-1* cDNA expressed under the control of the *rps-0* promoter (*Ex-cmtr-1*). Counts were performed on five individual animals per genotype.

568 **Loss of CMTR-1 does not affect spliced leader *trans*-splicing**

569 Approximately 85% of *C. elegans* genes produce transcripts that are *trans*-spliced to the
570 SL1 or SL2 spliced leaders (Tourasse et al., 2017), and both spliced leaders also
571 possess cOMe modifications (Figure 4E-G). In addition, we observed an interaction
572 between CMTR-1 and SNA-3, an essential component of the SL1 *trans*-splicing
573 machinery (Fasimoye et al, 2022, Eijlers et al, 2024) (Figure 3C). We therefore wanted to
574 investigate whether cOMe had any functional impact on *trans*-splicing. We depleted
575 mNG^AID::CMTR-1 in embryos by treating them with 5-Ph-IAA-AM, which is able to
576 penetrate the egg-shell (Negishi et al., 2022) and prepared *in vitro* splicing extracts as
577 described previously (Lasda et al., 2011). These were compared to extracts prepared
578 from untreated embryos, and to PE1220 embryos depleted for SNA-3::AID^mNG,
579 which, based on SNA-3's essential role, is predicted to impair spliced leader *trans*-
580 splicing (Fasimoye et al., 2022). 5-Ph-IAA-AM treatment reduced mNG^AID::CMTR-1
581 and SNA-3::mNG^AID steady-state levels to undetectable levels and by 80%,
582 respectively (Figure 5A).

583 We analysed the effect of protein depletion on spliced leader *trans*-splicing in
584 embryonic extracts using two assays: 1) the steady state spliced leader *trans*-splicing
585 levels of endogenous *rps-3* transcripts; and 2) the *trans*-splicing by embryonic extracts
586 of an exogenous, synthetic *rps-3* transcript prepared by *in vitro* transcription. In the first
587 assay, depletion of SNA-3 led to a 40.6-fold increase in non-*trans*-spliced, outron-
588 containing endogenous *rps-3* RNAs, while the depletion of CMTR-1 had only a minor
589 effect, leading to a 2.75-fold increase of non-*trans*-spliced *rps-3* RNA (Figure 5B).

590 SL1 *trans*-splicing of synthetic *rps-3* transcripts was analysed by PCR as previously
591 described (Lasda et al., 2011). The synthetic *rps-3* RNA used as substrate contains
592 plasmid sequence at the 3`-end allowing the use of primers that distinguish the
593 synthetic *rps-3* RNA from endogenous *rps-3* RNA (Figure 5C). Products P1, P2 and P3
594 (Figure 5C, D) were identified by sequence analysis and are detected by the SL-*rps-3*
595 primers that amplify SL *trans*-spliced synthetic RNA and the *rps-3* RNA control primers
596 that detect all forms of synthetic *rps-3* RNA. Importantly, SL-*rps-3* primer products
597 were only detected in reactions containing ATP necessary for spliced leader *trans*-
598 splicing to occur (Figure 5C). Analysis by qPCR shows that depletion of CMTR-1 has a
599 minor effect on *in vitro trans*-splicing of the exogenously added synthetic *rps-3* RNA,
600 with near-identical amounts of product detected in the presence of ATP, independent of
601 whether CMTR-1 was depleted or not (Figure 5D). In contrast, the depletion of SNA-3 led
602 to a 280-fold reduction of detection of *trans*-spliced products (Figure 5E). Thus, both
603 assays failed to detect a clear, pronounced effect of CMTR-1 depletion on spliced
604 leader *trans*-splicing, suggesting that neither cOMe nor CMTR-1 has a significant role in
605 this process.

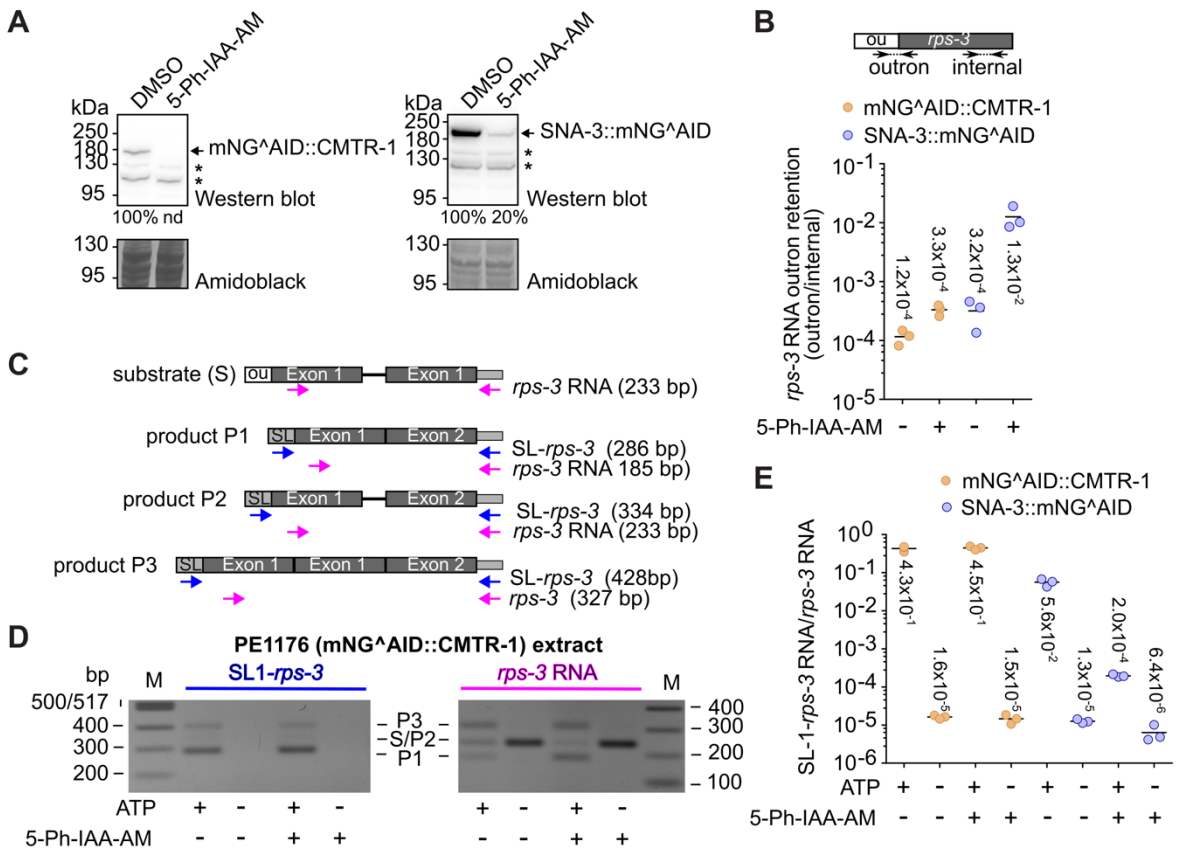

Figure 5. CMTR-1 is not required for spliced leader *trans*-splicing. (A) Western blots showing levels of endogenous mNG^AID::CMTR-1 and SNA-3::mNG^AID proteins in embryonic extracts prepared from PE1176 and PE1220 animals, respectively. Embryos were control-treated with DMSO or with the auxin analogue 5-Ph-IAA-AM for 4h prior to extract preparation. Proteins were analysed by Western blotting and detected by anti-mNeonGreen antibodies. Total protein visualised using amidoblack staining was used to standardise the levels of mNeonGreen-tagged proteins. The level of SNA-3::mNG^AID protein in 5-Ph-IAA-AM treated extract was expressed as percentage of that detected in the DMSO-treated extract. The mNG^AID::CMTR-1 was not detectable in 5-Ph-IAA-AM treated extracts (nd). Non-specific bands are indicated with a star symbol. (B) Quantitative RT-PCR measurement of outron retention of endogenous *rps-3* transcripts. The diagram shows the location of primers that detect outron and internal regions of *rps-3* RNA. RNA was isolated from embryonic extracts, reverse transcribed, and analysed by quantitative PCR as described previously (Philippe et al., 2017). The graph shows the ratio of endogenous *rps-3* outron to internal amplicon levels in PE1176 (gold) and PE1220 (blue) extracts treated with 5-Ph-IAA-AM (+) or control treated with

623 DMSO (-) determined using the ΔC_T method (Schmittgen and Livak, 2008).
624 Measurements are technical replicates and their means (horizontal line, mean values
625 are shown). The analysis is representative of 2 independent measurements. (C)
626 Substrate and products of *in vitro* SL *trans*-splicing. Diagrammatic representation of the
627 synthetic *rps-3* transcript (substrate S) with outron (ou) at the 5` end and the products
628 P1, P2 and P3. The locations of primer pairs SL1-*rps-3* and *rps-3* RNA used for detection
629 by one-step qPCR and expected amplicon size are indicated. (D) Analysis of *in vitro* SL
630 *trans*-splicing by agarose gel electrophoresis. Synthetic *rps-3* RNA was incubated with
631 embryonic extracts from PE1176 embryos treated with 5-Ph-IAA-AM or control-treated
632 with DMSO (+/- 5-Ph-IAA-AM) as described. ATP and ATP regeneration system were
633 included where indicated (+/- ATP). Products were amplified by one-step PCR, analysed
634 by 1.8% agarose gel electrophoresis and visualised by staining with ethidium bromide.
635 (E) Analysis of *in vitro* SL *trans*-splicing by quantitative RT-PCR. Synthetic *rps-3* RNA was
636 incubated with embryonic extracts from PE1176 (gold) or from PE1220 embryos (blue)
637 treated with 5-Ph-IAA-AM or control-treated with DMSO (+/- 5-Ph-IAA-AM) as described.
638 ATP and ATP regeneration system were included where indicated (+/- ATP). Products
639 were quantified by quantitative one-step RT-PCR as described. The graph shows the
640 ratio of *trans*-spliced SL1-*rps-3* products standardised with respect to total synthetic
641 *rps-3* RNA using the ΔC_T method (Schmittgen and Livak, 2008). The *in vitro* processing
642 reactions were done in triplicates. Shown are the results for each reaction and the
643 mean (horizontal line, values are indicated).

Loss of cOMe leads to differential transcript levels for genes involved in the intracellular pathogen response and germline sex determination

To investigate the possible impact of loss of cOMe on gene expression, we compared transcript levels for 5-Ph-IAA treated to control-treated animals. We cultured synchronised populations of mNG^AID::CMTR-1 larvae, and began the 5-Ph-IAA treatment when the animals were at the third larval (L3) stage, corresponding to the developmental stage at which CMTR-1 is critical for the sperm-oocyte switch (Figure 1J). Both control and 5-Ph-IAA treated animals were harvested for RNA preparation at early L4 stage.

We performed differential gene expression analysis, comparing RNA-Seq derived from control versus 5-Ph-IAA treated animals. This revealed 1953 genes whose steady state transcript levels were significantly upregulated by mNG^AID::CMTR-1 depletion (FDR<=0.05, absolute log2 fold change >=1), and 3398 genes for which transcript levels were significantly reduced by the same treatment (FDR<=0.05, absolute log2 fold change >=1) (Supplementary Table 3).

Inspection of the genes that were significantly enriched more than four-fold in mNG^AID::CMTR-1 knock-down worms compared to controls revealed upregulation of around 80 genes, including *fbxa-158*, *pals-14*, and *pals-6*, which belong to a class of genes that constitute the intracellular pathogen response (IPR), a *C. elegans* transcriptional immune response to intracellular pathogens (Lažetić et al., 2023). IPR is induced by viral and microsporidia infections, but also mitochondrial dysfunction(Mao et al., 2022; Sowa et al., 2020).

666 To systematically investigate the possibility that IPR genes were generally upregulated in
667 response to depletion of CMTR-1, we extracted the fold changes of 272 IPR genes that
668 were upregulated more than four-fold in response to expression of Orsay virus RNA-
669 dependent RNA polymerase (Sowa et al., 2020)(Figure 6A). These IPR genes showed
670 statistically significantly higher transcript levels in response to CMTR-1 depletion
671 compared to non-IPR genes ($P<<0.001$), though the effect size was modest (mean fold
672 change: 0.697) (Figure 6A). The effect of loss of CMTR-1 on innate immune gene
673 expression was also supported by GeneOntology (GO) term enrichment analysis (Figure
674 6B): the three most significantly overrepresented GO terms among upregulated genes
675 were "innate immune response" (GO:0045087, qvalue = 2.02×10^{-8}), "response to
676 external biotic stimulus" (GO:0043207, qvalue = 3.92×10^{-7}), and "defense response"
677 (GO:0006952, qvalue = 4.20×10^{-7}). Thus, loss of CMTR-1 and cOMe leads to
678 transcriptional upregulation of many intracellular pathogen response genes.

679 GO term enrichment analysis among downregulated genes in response to loss of CMTR-
680 1 highlighted a broad range of metabolic terms but, intriguingly, also terms related to
681 gametogenesis, including "gamete generation" (GO:0007276, qvalue = 3.59×10^{-13}) and
682 "germ cell development" (GO:0007281, qvalue = 1.96×10^{-9}) (Supplementary Table 3).

683 To investigate whether transcripts from genes associated with germline sex
684 determination were downregulated in response to depletion of CMTR-1, we extracted
685 the fold changes of a set of 64 genes involved in germline sex determination (Figure 6A).
686 We found that this set of genes showed statistically significantly ($P<<0.001$) lower fold
687 changes than all other genes, though as for the IPR gene response, the effect size was
688 modest (mean fold change: -0.287). Nonetheless, since germline development is

689 known to be highly sensitive to shifts in gene expression (Ellis, 2022), this overall trend

690 of downregulation may explain the germline defects that we observed (Figure 1).

691 We were unable to establish a clear correlation between transcript level changes and

692 the growth defects that we observe in animals depleted of CMTR-1. It is likely that

693 changes in the expression of a broad range of genes are responsible for this phenotype.

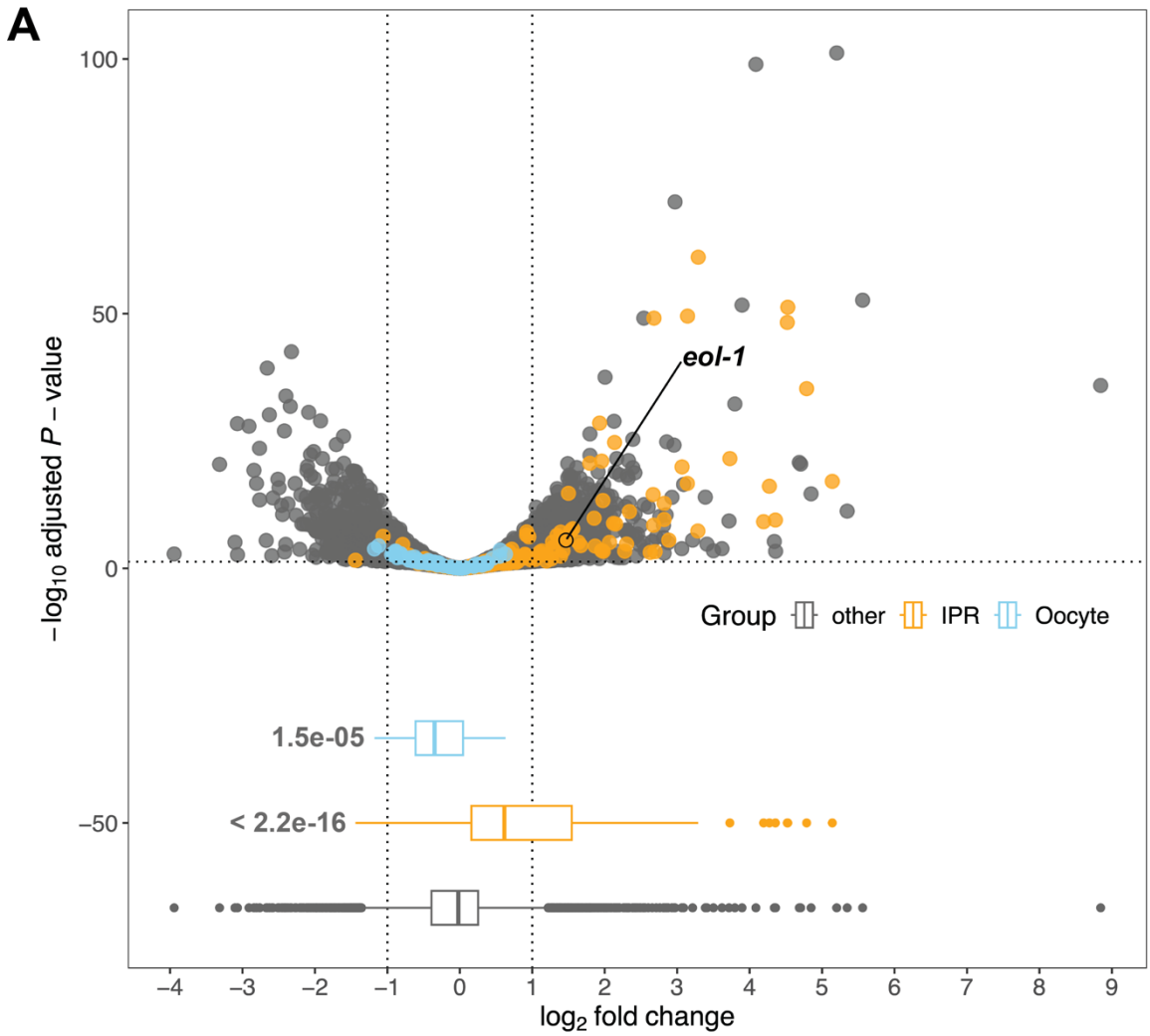
A
100
50
0
−50
−log10 adjusted P − value
eol-1
Group
other
IPR
Oocyte
1.5e-05
< 2.2e-16
−4
−3
−2
−1
0
1
2
3
4
5
6
7
8
9
log2 fold change

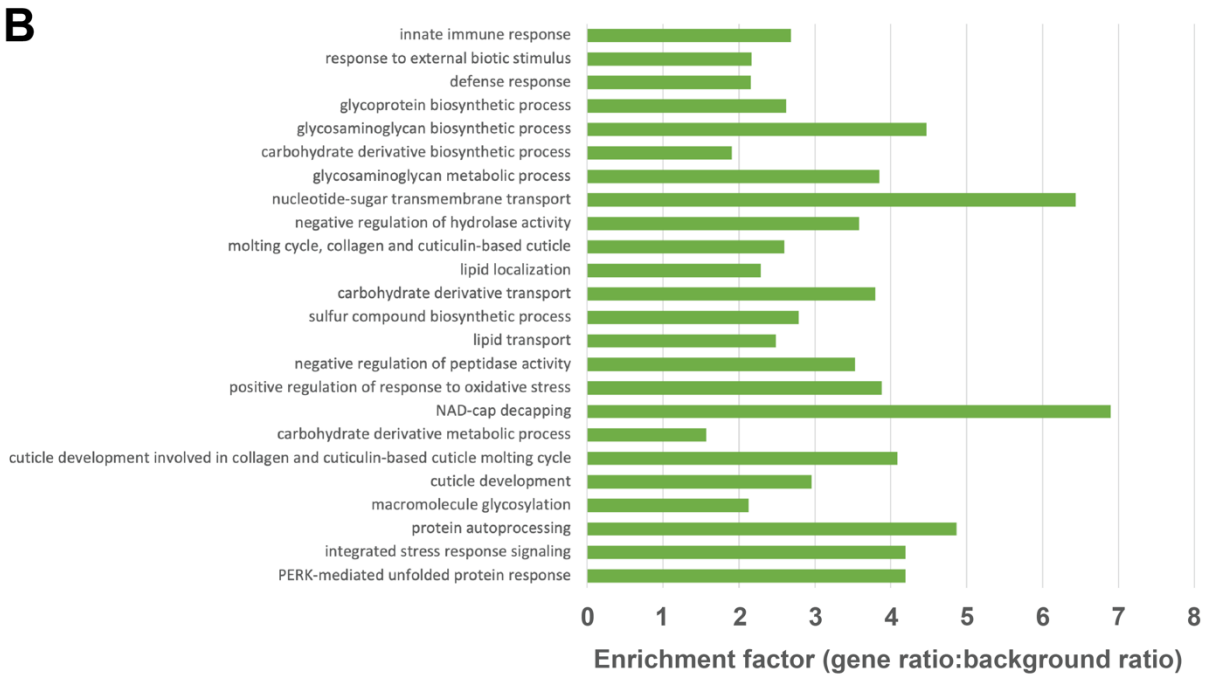
B
innate immune response
response to external biotic stimulus
defense response
glycoprotein biosynthetic process
glycosaminoglycan biosynthetic process
carbohydrate derivative biosynthetic process
glycosaminoglycan metabolic process
nucleotide-sugar transmembrane transport
negative regulation of hydrolase activity
molting cycle, collagen and cuticulin-based cuticle
lipid localization
carbohydrate derivative transport
sulfur compound biosynthetic process
lipid transport
negative regulation of peptidase activity
positive regulation of response to oxidative stress
NAD-cap decapping
carbohydrate derivative metabolic process
cuticle development involved in collagen and cuticulin-based cuticle molting cycle
cuticle development
macromolecule glycosylation
protein autoprocessing
integrated stress response signaling
PERK-mediated unfolded protein response
0
1
2
3
4
5
6
7
8
Enrichment factor (gene ratio:background ratio)

694

Figure 6. Depletion of CMTR-1 results in upregulation of transcripts associated with the innate immune response and downregulation of transcripts involved in germline sex determination. (A) Upper panel, volcano plot showing differential gene expression in animals subject to CMTR-1 depletion compared to controls (three biological replicates). Intracellular pathogen response genes (IPR) are highlighted in orange. Germline sex determination genes (Oocyte) are highlighted in blue. Lower panel, box plot of the fold change data, showing the p-values (Welch Two Sample t-test) for the differences between the means of the IPR and Oocyte gene sets and the "other" (non-IPR/germline sex determination genes). The gene *eol-1*, which is part of the IPR and was subsequently shown in this study to be epistatic to *cmtr-1* (Figure 7), is also indicated. (B) Gene ontology enrichment analysis showing the significantly enriched gene categories among upregulated genes in animals subject to CMTR-1 depletion compared to controls ranked by q-value.

708 **Loss of the RNA decapping exonuclease EOL-1 bypasses the need for CMTR-1**

709 To better understand the molecular and cellular significance of the global loss of cOMe,
710 we performed an unbiased screen for suppressors of the *cmtr-1* loss-of-function
711 phenotype, reasoning that such mutations might allow us to identify components
712 involved in the cellular response to cOMe modified RNAs.

713 We mutagenised PE1176 worms with ethyl methanesulfonate (EMS) and grew the F2
714 generation on NGM plates containing 1 μM 5-Ph-IAA. We then screened for the
715 presence of healthy gravid worms, which would indicate suppression of the *cmtr-1* loss-
716 of-function phenotype. Suppression was confirmed by showing that the worms could
717 be maintained over multiple generations on 5-Ph-IAA containing media. Only one strain
718 was retained per F1 culture, to ensure independence of each suppressor mutation.
719 From combined screens of approximately 20,000 haploid genomes, we recovered 27
720 independent mutants that were fertile when grown in the presence of 5-Ph-IAA.

721 We designed the screen with the expectation that we would recover loss of function
722 mutations in the *TIR1(F79G)* transgene, which restore fertility simply by preventing 5-Ph-
723 IAA-depdenent degradation of mNG^AID ::CMTR-1. Such mutations, which constitute a
724 type of informational suppression (Mount and Anderson, 2000), could be distinguished
725 from *bona fide cmtr-1* loss-of-function suppressors by the fact that they express
726 mNG::AID^CMTR-1 in the presence of 5-Ph-IAA (Supplementary Figure 2). Using this
727 secondary screen, we found that of the 27 mutants, 21 showed nuclear mNeonGreen
728 fluorescence despite being grown on 5-Ph-IAA. We sequenced the TIR1 coding region
729 from six of the putative TIR1 loss-of-function mutants and confirmed that all were
730 missense mutations (Supplementary Figure 2).

731 The six mutants that lacked mNeonGreen fluorescence but were nonetheless fertile
732 were thus putative suppressors that bypass the requirement for CMTR-1. We confirmed
733 that they also suppressed the *cmtr-1(syb3613)* null allele: all six mutations suppressed
734 the sterile phenotype and growth defects conferred by the *syb3613* allele confirming
735 that they are epistatic to *cmtr-1* loss-of-function (Figure 7A).

736 To identify the gene(s) affected by these six mutations, we used a whole-genome
737 sequencing (WGS) mapping strategy based on the sibling-subtraction approach
738 described previously (Joseph et al., 2017). We mapped two of the suppressor mutants,
739 *fe152* and *fe154*, using this approach (Supplementary Figure 3). The sibling-subtraction
740 WGS mapping approach relies on the identification of variants that are present in more
741 than 90% of reads derived from the pooled broods of F2 suppressor animals, but
742 absent, or at a low frequency in the reads derived from their non-suppressor sibling
743 broods. In practice, we found that focussing only on variants found in 100% of
744 suppressor pool reads was sufficient to narrow down the location of the suppressor
745 mutations to a region of chromosome V (Supplementary Table 4). SnpEff and manual
746 curation of these variants revealed predicted damaging variants in a single gene, *eol-1*,
747 allowing us to assign *fe152* and *fe154* as premature stop codon mutations, W208Opal
748 and W211Amber, respectively (Figure 7B).

749 Sanger sequencing of the *eol-1* locus in the other four suppressor mutants revealed that
750 each was a predicted damaging allele of *eol-1* (Figure 7B). A third nonsense mutation is
751 created by *fe174*, R168Opal, and two mutations, *fe155* and *fe172*, are missense
752 mutations, C162Y and E297K, respectively. The *fe153* allele was found to be a deletion
753 of 1456 bp that removes 940 bp upstream of the start codon as well as half of the

754 coding region. The deletion is accompanied by insertion of 349 bp of sequence, part of
755 which appears to be repetitive DNA found on multiple *C. elegans* chromosomes.

756 Having identified the genetic location of the suppressor mutations, we crossed them
757 into a *cmtr-1* wild-type background, which revealed that they had wild-type brood sizes
758 (Figure 7A). Thus, loss of *eol-1* function is compatible with wild-type fertility. We also did
759 not detect any obvious phenotypes that would indicate defects in embryonic or
760 postembryonic development.

761 Although the recovery of six independent function altering mutations in the same gene
762 is strong evidence that loss of *eol-1* function suppresses the requirement for CMTR-1
763 and thus cOMe, we wanted to formally confirm this. We aimed to delete the *eol-1* gene,
764 using Cas9/CRISPR to generate double-strand breaks at either end of the gene.
765 However, we found that the guide RNA targeted to the 5`-end of the coding region was
766 ineffective, so we were not able to identify gene deletions. Nonetheless, we identified
767 two alleles, *fe176* and *fe177*, that created frameshifts just upstream of the stop codon,
768 both of which would be predicted to result in peptide extensions that derive from
769 translation into the 3`-UTR (Figure 7B). Proteins with such C-terminal extensions are
770 subject to "readthrough mitigation" mechanisms that lead to downregulation of the
771 affected protein (Arribere et al., 2016; Kesner et al., 2023; Müller et al., 2023).
772 Consistent with this, both alleles suppress the sterile phenotype caused by depletion of
773 CMTR-1, confirming that loss of *eol-1* function bypasses the requirement for cOMe.

774 EOL-1 is a member of the DXO/Rai1 family of decapping enzymes (Chang et al., 2012;
775 Jiao et al., 2013; Mao et al., 2020; Shen et al., 2014), and some members are also
776 distributive 5` to 3` exonucleases, so that they can both decap and degrade their target

RNAs. The missense mutations, C162Y and E297K, alter residues that are part of the predicted active site of EOL-1 (Figure 7C). Indeed, E297 is the homologue of mammalian DXO E253, a critical catalytic residue, part of the so-called Motif IV (Chang et al., 2012; Jiao et al., 2013). Thus EOL-1 loss of function mutations which specifically abolish its decapping/exonuclease activity, completely suppress the sterility caused by loss of CMTR-1, indicating that removing this activity is likely the mechanism which mediates the suppression.

Previous studies have shown that EOL-1 is a prominent part of the intracellular pathogen response. Given that loss of CMTR-1 led to enrichment of transcripts associated with this response, we looked for evidence that *eol-1* transcripts are enriched in CMTR-1 depleted animals compared to controls (Figure 6A) and found that they are enriched 2.76-fold. EOL-1 is one of nine *C. elegans* DXO homologues (Mao et al., 2020), and is part of a clade of paralogues (Figure 7D). Transcripts from four of these are also upregulated by depletion of CMTR-1, though only two of them are broadly upregulated as part of the intracellular pathogen response (Supplementary Table 3).

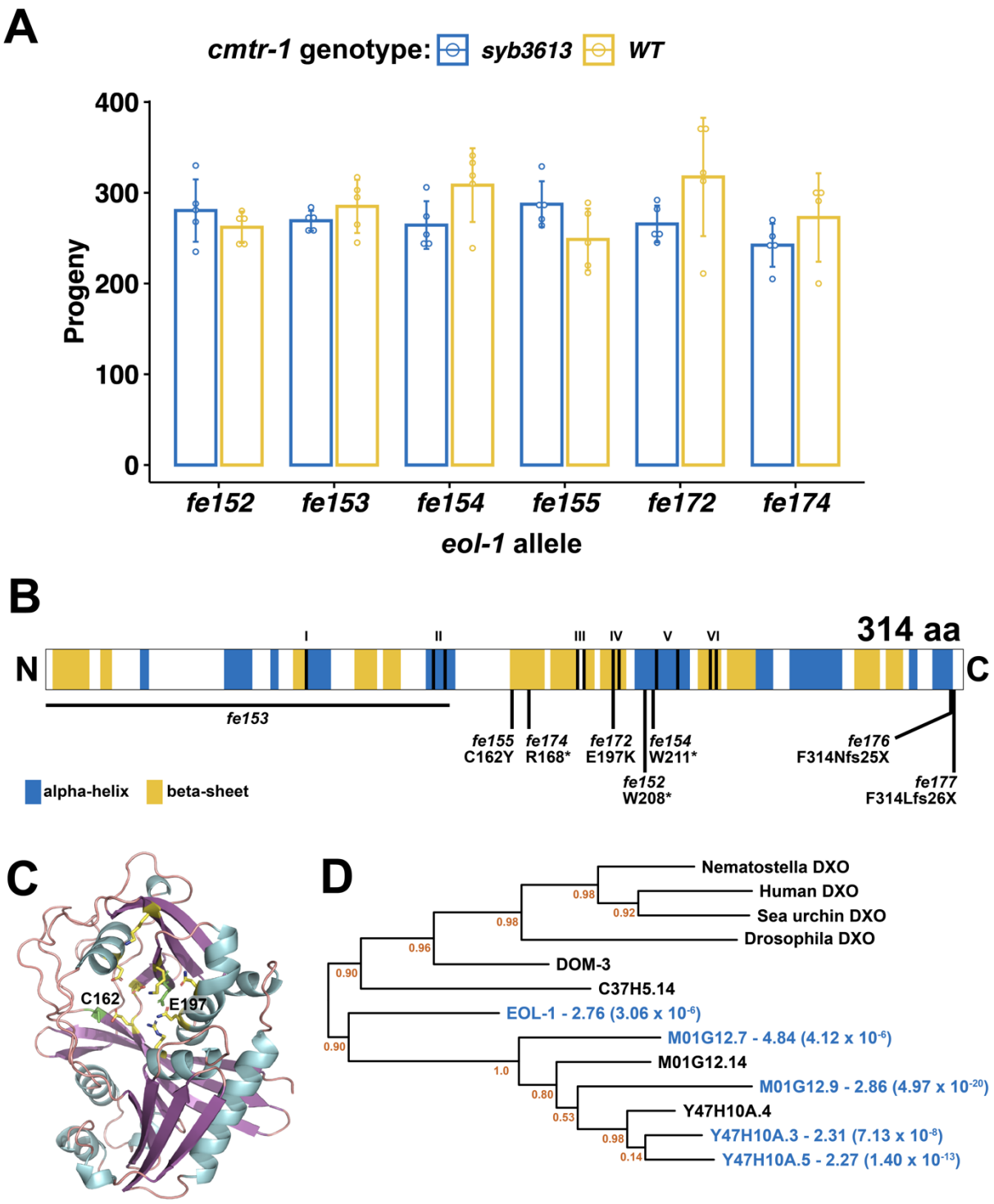

Figure 7. Loss of function mutations in *eol-1* suppress the loss of *cmtr-1* mutant phenotype. (A) Brood counts for the six *eol-1* alleles identified as suppressors of *cmtr-1* loss-of-function in *cmtr-1(syb3613)* and *cmtr-1(+)* backgrounds. Histograms show means and error bars show standard deviations for counts derived from five adults for

each genotype. (B) Schematic of EOL-1 showing the location of the suppressor mutations and the two mutations generated by Cas9/CRISPR (*fe176* and *fe177*). Shading indicates secondary structure assignments based on the AlphaFold prediction (A5JYX9). Roman numerals indicate highly conserved motifs necessary for decapping and exonuclease activity (Wang et al., 2015). (C) AlphaFold prediction for EOL-1, showing location of residues affected by missense suppressor mutations (green). Active site residues other than E197 are in yellow. (D) Phylogram showing the relationship between EOL-1 and other DXO family members. Blue text indicates proteins with transcripts that are significantly enriched in mNG^AID::CMTR-1 depleted animals. Fold enrichment is given, along with adjusted *p* values in brackets. Node statistical supports are given as aLRT (SH-like) values.

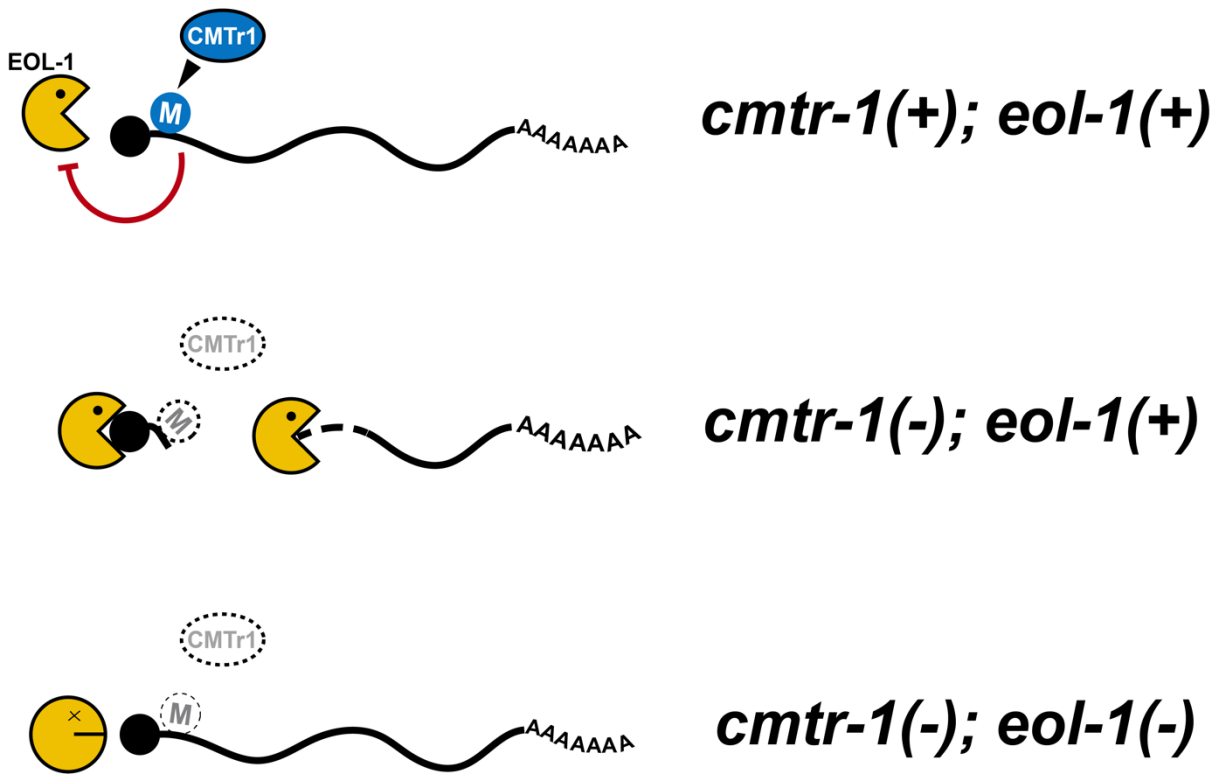

Figure 8. Cap-adjacent 2`-O-ribose methylation protects cellular transcripts from EOL-1-mediated degradation. In this proposed model, EOL-1 is prevented from decapping cOMe modified transcripts (M). In the absence of CMTR-1, transcripts lack cOMe and thus become substrates for EOL-1. Transcripts for genes that are sensitive to copy number changes, such as those involved in germline cell fate, would be most susceptible to loss of cOMe. Loss of EOL-1 prevents the degradation of these transcripts. Black shaded circle indicates the monomethyl guanosine cap.

DISCUSSION

Insights into the role of cOMe in animal development requires that one study the effects of loss of the CMTR proteins in the context of whole organism biology. While work in mice and flies have advanced our understanding of cOMe biology, the fact that these RNA modifications are essential for mammalian embryogenesis, but dispensable in flies and some cultured mammalian cells is puzzling. By investigating cOMe function in *C. elegans*, we have obtained a broader evolutionary perspective of the role of these RNA modifications.

Unlike the situation in mammals (Furuichi et al., 1975; Werner et al., 2011), we find that CMTR-1 is the principal enzyme involved in adding cOMe to *C. elegans* RNAs, and consistent with this, has higher steady state nuclear levels compared to CMTR-2. Similarly consistent with these observations, CMTR-1 is essential while CMTR-2 is not. We did not find a function for CMTR-2 beyond augmenting that of CMTR-1, which suggests that CMTR-2 is also able to modify the first nucleotide, a substrate specificity also found for its *Drosophila* and human homologues in modifying canonical AGU starting transcripts (Anreiter et al., 2020; Dix et al., 2022; Haussmann et al., 2022).

The two nematode CMTR proteins have distinct sub-cellular localisations and interaction partners, suggesting that they are functionally differentiated. Much of this may be due to their differing subcellular localisations. As in mammals and *Drosophila* (Haussmann et al., 2022; Werner et al., 2011), we see stronger associations of CMTR-2 with the cytoplasm. This is most pronounced during embryogenesis where CMTR-2 is apparently excluded from the nucleus, something not reported in other animal cells. This observation warrants further investigation.

840 The protein interaction profile of *C. elegans* CMTR-1 is highly similar to its mammalian
841 homologue (Simabuco et al., 2019), with both proteins showing prominent interactions
842 with the spliceosome. The functional significance of these observations is unclear but
843 may simply reflect the fact that these proteins assemble on nascent transcripts, though
844 we cannot rule out a functional role for CMTR-1 in *cis*-splicing of certain transcripts.
845 However, our experiments do indicate that CMTR-1 is not an essential component of
846 nematode spliced leader *trans*-splicing. Despite the interaction between CMTR-1 and
847 SNA-3, neither of our functional assays indicates that CMTR-1 is required for the activity
848 of the *trans*-spliceosome.

849 **A role for EOL-1 in degrading RNAs lacking cap-adjacent 2`-O-ribose methylation**

850 Since cOMe plays an essential physiological role in *C. elegans*, this has allowed us to
851 fully exploit the advantages of this genetically tractable model system to understand the
852 mechanistic basis of the cellular response to cOMe. Importantly, we have identified
853 EOL-1 as a key effector that recognises transcripts lacking cOMe. A previous study
854 showed that cOMe blocks the activity of mammalian DXO *in vitro* (Picard-Jean et al.,
855 2018). The genetic interaction between *cmtr-1* and *eol-1* demonstrates that this
856 interaction is physiologically significant. Since we find that loss of EOL-1 effectively
857 bypasses the requirement for CMTR-1, and hence cOMe, our work provides clear
858 support for the hypothesis that DXO proteins recognise and destroy RNAs that lack
859 cOMe (Figure 8). Thus, in animals lacking CMTR-1, all cellular transcripts become
860 potential targets, leading to changes in steady-state transcript levels that we see
861 correlated with defects in germline development.

862 What is the physiological significance of EOL-1 activity? In wild-type animals, most, if
863 not all, RNA polymerase II transcripts will possess this modification and thus would be
864 protected from EOL-1 degradation. Previous studies have proposed that DXO proteins
865 maintain RNA quality control, removing partially capped RNAs that lack cOMe before
866 they enter the cytoplasm (Jiao et al., 2013). They have also been shown to have a high
867 affinity for NAD-capped RNAs, which are targeted by DXO for rapid degradation
868 (Kiledjian, 2018). Such roles would be consistent with our data. However, since EOL-1 is
869 a prominent component of the intracellular pathogen response, a role in innate
870 immunity is also plausible; indeed, previous studies of this protein show that it is
871 intimately associated with responses to pathogens and cellular dysfunction.

872 EOL-1 was first identified in screens for mutants with enhanced aversive behavioural
873 responses to pathogenic bacteria (Shen et al., 2014), and it is a notable member of the
874 intracellular pathogen response, induced by Orsay virus, a positive sense, single-
875 stranded RNA virus, and the microsporidian *Nematocida parisii* (Chen et al., 2017; Tecle
876 et al., 2021). Mutations associated with mitochondrial dysfunction also result in
877 elevated *eol-1* expression levels (Mao et al., 2020; Senchuk et al., 2018), and EOL-1
878 protein undergoes changes in its intracellular localisation, forming cytoplasmic foci in
879 response to mitochondrial defects (Mao et al., 2020). However, a mechanistic role for
880 EOL-1 in innate immunity has yet to be defined. Our work connecting EOL-1 to cOMe
881 suggests a possible function for this protein in the surveillance for RNAs lacking cap1
882 structures. Mitochondrial dysfunction leads to the presence of RNAs in the cytoplasm
883 that lack cOMe (Mao et al., 2020), which would presumably be substrates for EOL-1
884 degradation. Moreover, mitochondrial RNAs also possess high levels of NAD-caps,
885 making them preferential DXO family substrates (Bird et al., 2018; Jiao et al., 2017).

886 Likewise, Orsay virus RNAs, for instance, lack both a 5` monomethyl guanosine cap and
887 cOMe modifications (Ashe et al., 2013). Thus, the identification and removal of
888 pathogenic RNAs on the basis of cOMe absence is a plausible function of this enzyme
889 in *C. elegans* that warrants further exploration.

890 The relationship we have discovered between cOMe and EOL-1 may have broader
891 phylogenetic significance, with DXO proteins having a conserved role in RNA
892 surveillance based on cOMe status. In particular, this may explain the molecular basis
893 of the lethality observed in mammalian embryos lacking either of the two CMTRs
894 (Dohnalkova et al., 2023); in the light of our work, perhaps loss of cOMe in mouse
895 embryos renders many cellular transcripts targets of mammalian DXO. While *DXO*
896 transcripts are not upregulated by the loss of cOMe (Dohnalkova et al., 2023), unlike
897 those of *eol-1* in *C. elegans*, cellular levels of DXO may still be sufficient to have an
898 impact across the transcriptome. Thus, the embryonic lethality observed in embryos
899 lacking cOMe might be explained by the cumulative downregulation of multiple
900 transcripts. It will be important to determine whether loss of DXO can suppress the
901 embryonic lethality of loss of *Cmtr1* in mice.

902 **Cap-adjacent 2`-O-ribose methylation and the innate immune response**

903 Our findings highlight similarities between the functions of cOMe in nematodes and
904 mammals: as in mammals, loss of cOMe leads to the upregulation of genes associated
905 with an innate transcriptional immune response. This raises the possibility that cOMe is
906 a determinant that regulates an RNA-mediated immune response in *C. elegans*. The
907 upregulation of IPR genes that we observed in animals depleted of CMTR-1 is intriguing
908 given that loss of CMTR1 in mammals also results in induction of the innate immune

909 response (Daffis et al., 2010; Dohnalkova et al., 2023; Schuberth-Wagner et al., 2015).
910 In mammals, RNAs lacking cOMe are directly sensed by RIG-I, which binds to double-
911 stranded RNA substrates that lack cOMe and leads to the activation of the type I
912 interferon response (Devarkar et al., 2016; Schuberth-Wagner et al., 2015); although the
913 mechanism by which cellular RNAs are converted into double-stranded RNAs remains
914 unclear.

915 In *C. elegans*, there are three RIG-I homologues, DRH-1, DRH-2 and DRH-3 (Guo et al.,
916 2013), but DRH-1 appears to be functionally most similar to RIG-I in that it recognises
917 viral RNAs and is essential for the intracellular pathogen response to viral infection
918 (Sowa et al., 2020). Indeed, the double-stranded RNA sensing module (the helicase and
919 C-terminal domains) of RIG-I can functionally substitute for the homologous region of
920 DRH-1 in assays for viral load (Guo et al., 2013); and native DRH-1 binds to double-
921 stranded RNAs in a manner similar to RIG-I (Consalvo et al., 2024). Thus, if the
922 upregulation of the intracellular pathogen response is a direct effect of appearance of
923 RNAs lacking cOMe, then DRH-1is a good candidate involved in their detection; it will be
924 important to test whether loss of *drh-1* results in abrogation of the intracellular
925 pathogen response in animals lacking cOMe.

926 An alternative possibility is that the induction of the intracellular pathogen response by
927 loss of cOMe is indirect, caused by the overall impact that this loss has on global gene
928 expression patterns. The intracellular pathogen response is also induced by proteotoxic
929 stress (Bakowski et al., 2014; Panek et al., 2020; Reddy et al., 2017), so the global,
930 cumulative effects on gene expression caused by loss of cOMe, might lead to an
931 intracellular pathogen response due to disruption of proteostasis. Distinguishing

932 between direct and indirect effects of cOMe on the transcriptional immune response in
933 *C. elegans* will be important in determining the extent of functional conservation of
934 cOMe function between nematodes and mammals.

935 Multiple studies in diverse experimental systems have described roles for cOMe at
936 multiple steps in the regulation of gene expression, including transcription, splicing and
937 translation (Dönmez et al., 2004; Drazkowska et al., 2022; Haussmann et al., 2022; Kuge
938 et al., 1998; Liang et al., 2022; Yu et al., 1998). It is thus surprising that in *C. elegans* that
939 lack EOL-1, cOMe is largely dispensable, at least in laboratory culture. However, our
940 results are consistent with work showing that in certain mammalian cell types, the
941 impact of loss of cOMe is relatively minor (Dohnalkova et al., 2023). Similarly, loss of
942 cOMe in *Drosophila* does not result in profound cellular impacts, with such animals
943 being viable and fertile (Haussmann et al., 2022). The ubiquity of cOMe and the
944 conservation of the two CMTR proteins that catalyse it shows that it must have an
945 essential role across animal phylogeny. Perhaps its original, ancestral role was in RNA-
946 based immune surveillance, which has been preserved in *C. elegans* and mammals
947 (but apparently lost in *Drosophila*), with its functions in gene expression having arisen
948 due cellular adaptation to the presence of cOMe on cellular RNAs. Alternatively, it may
949 have been co-opted into roles in innate immunity through convergent evolution in
950 mammals and nematodes from an ancestral function(s) in the regulation of gene
951 expression. Better understanding of the molecular impacts of cOMe loss in diverse
952 physiologically relevant experimental systems will be needed to distinguish these
953 hypotheses.

954

DATA AVAILABILITY

The mass spectrometry proteomics data have been deposited to the ProteomeXchange Consortium via the PRIDE (Perez-Riverol et al., 2022) partner repository with the dataset identifier PXD058991 (See also Supplementary Table 2). The RNA-Seq data used for the CMTR-1 depletion differential gene expression analysis have been deposited in ArrayExpress under accession number E-MTAB-14816. Sequence reads that were used in the sibling selection whole genome sequence mapping of *eol-1(fe152)* and *eol-1(fe154)* are available in the NCBI Sequence Read Archive under BioProject ID PRJNA1216994.

ACKNOWLEDGEMENTS

We thank Omar Alotaibi, Holly Armstrong, Sandeep Goli, Phurichaya Khunthong, and Ursula Terech Rial for their assistance with the *cmtr-1* suppressor screen. We also thank Max Bracken-Zmuda for help making the *cmtr-1(feK244A)* strain. Some strains were provided by the Caenorhabditis Genetics Center, which is funded by NIH Office of Research Infrastructure Programs (P40 OD010440). Proteomic analysis was performed by Aberdeen Proteomics, and we thank Kate Burgoyne and Craig Pattinson for technical support. We thank WormBase for providing the community resource that facilitated the interrogation of *C. elegans* molecular genetics used in this work. We acknowledge the support of the Maxwell HPC computer cluster funded by the University of Aberdeen. This work was supported by the UKRI Biotechnology and Biological Sciences Research Council (BBSRC) grant number BB/T00875X/1.

977 **REFERENCES**

978 Adams JM, Cory S. 1975. Modified nucleosides and bizarre 5`-termini in mouse
979 myeloma mRNA. *Nature* **255**:28–33.
980 Andrews S. 2010. FastQC: a quality control tool for high throughput sequence data.
981 https://www.bioinformatics.babraham.ac.uk/projects/fastqc/
982 Anreiter I, Mir Q, Simpson JT, Janga SC, Soller M. 2020. New Twists in Detecting mRNA
983 Modification Dynamics. *Trends Biotechnol*. doi:10.1016/j.tibtech.2020.06.002
984 Anreiter I, Tian YW, Soller M. 2023. The cap epitranscriptome: Early directions to a
985 complex life as mRNA. *Bioessays* **45**:e2200198.
986 Arribere JA, Bell RT, Fu BXH, Artiles KL, Hartman PS, Fire AZ. 2014. Efficient marker-free
987 recovery of custom genetic modifications with CRISPR/Cas9 in *Caenorhabditis*
988 *elegans*. *Genetics* **198**:837–846.
989 Arribere JA, Cenik ES, Jain N, Hess GT, Lee CH, Bassik MC, Fire AZ. 2016. Translation
990 readthrough mitigation. *Nature* **534**:719–723.
991 Ashburner M, Ball CA, Blake JA, Botstein D, Butler H, Cherry JM, Davis AP, Dolinski K,
992 Dwight SS, Eppig JT, Harris MA, Hill DP, Issel-Tarver L, Kasarskis A, Lewis S,
993 Matese JC, Richardson JE, Ringwald M, Rubin GM, Sherlock G. 2000. Gene
994 ontology: tool for the unification of biology. The Gene Ontology Consortium. *Nat*
995 *Genet* **25**:25–29.
996 Ashe A, Bélicard T, Le Pen J, Sarkies P, Frézal L, Lehrbach N, Félix M, Miska E. 2013. A
997 deletion polymorphism in the *Caenorhabditis elegans* RIG-I homolog disables
998 viral RNA dicing and antiviral immunity. *Elife* **2**. doi:10.7554/eLife.00994

999 Bakowski MA, Desjardins CA, Smelkinson MG, Dunbar TL, Lopez-Moyado IF, Rifkin SA,
1000 Cuomo CA, Troemel ER. 2014. Ubiquitin-mediated response to microsporidia
1001 and virus infection in *C. elegans*. *PLoS Pathog* **10**:e1004200.
1002 Bélanger F, Stepinski J, Darzynkiewicz E, Pelletier J. 2010. Characterization of hMTr1, a
1003 human Cap1 2`-O-ribose methyltransferase. *J Biol Chem* **285**:33037–33044.
1004 Benjamini Y, Hochberg Y. 1995. Controlling the false discovery rate: A practical and
1005 powerful approach to multiple testing. *J R Stat Soc Series B Stat Methodol*
1006 **57**:289–300.
1007 Bird JG, Basu U, Kuster D, Ramachandran A, Grudzien-Nogalska E, Towheed A, Wallace
1008 DC, Kiledjian M, Temiakov D, Patel SS, Ebright RH, Nickels BE. 2018. Highly
1009 efficient 5` capping of mitochondrial RNA with NAD+ and NADH by yeast and
1010 human mitochondrial RNA polymerase. *Elife* **7**. doi:10.7554/eLife.42179
1011 Chang JH, Jiao X, Chiba K, Oh C, Martin CE, Kiledjian M, Tong L. 2012. Dxo1 is a new type
1012 of eukaryotic enzyme with both decapping and 5`-3` exoribonuclease activity.
1013 *Nat Struct Mol Biol* **19**:1011–1017.
1014 Chen K, Franz CJ, Jiang H, Jiang Y, Wang D. 2017. An evolutionarily conserved
1015 transcriptional response to viral infection in Caenorhabditis nematodes. *BMC*
1016 *Genomics* **18**:303.
1017 Cingolani P, Platts A, Wang LL, Coon M, Nguyen T, Wang L, Land SJ, Lu X, Ruden DM.
1018 2012. A program for annotating and predicting the effects of single nucleotide
1019 polymorphisms, SnpEff. *Fly (Austin)* **6**:80–92.
1020 Consalvo CD, Aderounmu AM, Donelick HM, Aruscavage PJ, Eckert DM, Shen PS, Bass
1021 BL. 2024. *Caenorhabditis elegans* Dicer acts with the RIG-I-like helicase DRH-1
1022 and RDE-4 to cleave dsRNA. *Elife* **13**. doi:10.7554/eLife.93979

1023 Daffis S, Szretter KJ, Schriewer J, Li J, Youn S, Errett J, Lin T-Y, Schneller S, Zust R, Dong
1024 H, Thiel V, Sen GC, Fensterl V, Klimstra WB, Pierson TC, Buller RM, Gale M Jr, Shi
1025 P-Y, Diamond MS. 2010. 2`-O methylation of the viral mRNA cap evades host
1026 restriction by IFIT family members. *Nature* **468**:452–456.
1027 Danecek P, Bonfield JK, Liddle J, Marshall J, Ohan V, Pollard MO, Whitwham A, Keane T,
1028 McCarthy SA, Davies RM, Li H. 2021. Twelve years of SAMtools and BCFtools.
1029 *Gigascience* **10**:giab008.
1030 DeMott E, Dickinson D, Doonan R. 2021. Highly improved cloning efficiency for plasmid-
1031 based CRISPR knock-in in *C. elegans*. *MicroPubl Biol* **2021**.
1032 doi:10.17912/micropub.biology.000499
1033 Despic V, Jaffrey SR. 2023. mRNA ageing shapes the Cap2 methylome in mammalian
1034 mRNA. *Nature* **614**:358–366.
1035 Devarkar SC, Wang C, Miller MT, Ramanathan A, Jiang F, Khan AG, Patel SS,
1036 Marcotrigiano J. 2016. Structural basis for m7G recognition and 2`-O-methyl
1037 discrimination in capped RNAs by the innate immune receptor RIG-I. *Proc Natl*
1038 *Acad Sci U S A* **113**:596–601.
1039 Dickinson DJ, Pani AM, Heppert JK, Higgins CD, Goldstein B. 2015. Streamlined Genome
1040 Engineering with a Self-Excising Drug Selection Cassette. *Genetics* **200**:1035–
1041 1049.
1042 Dix TC, Haussmann IU, Brivio S, Nallasivan MP, HadzHiev Y, Müller F, Müller B, Pettitt J,
1043 Soller M. 2022. CMTr mediated 2`-O-ribose methylation status of cap-adjacent
1044 nucleotides across animals. *RNA* **28**:1377–1390.
1045 Dohnalkova M, Krasnykov K, Mendel M, Li L, Panasenko O, Fleury-Olela F, Vågbø CB,
1046 Homolka D, Pillai RS. 2023. Essential roles of RNA cap-proximal ribose

1047 methylation in mammalian embryonic development and fertility. *Cell Rep*
1048 **42**:112786.
1049 Doitsidou M, Poole RJ, Sarin S, Bigelow H, Hobert O. 2010. *C. elegans* mutant
1050 identification with a one-step whole-genome-sequencing and SNP mapping
1051 strategy. *PLoS One* **5**:e15435.
1052 Dönmez G, Hartmuth K, Lührmann R. 2004. Modified nucleotides at the 5` end of
1053 human U2 snRNA are required for spliceosomal E-complex formation. *RNA*
1054 **10**:1925–1933.
1055 Drazkowska K, Tomecki R, Warminski M, Baran N, Cysewski D, Depaix A, Kasprzyk R,
1056 Kowalska J, Jemielity J, Sikorski PJ. 2022. 2'-O-Methylation of the second
1057 transcribed nucleotide within the mRNA 5'`cap impacts the protein production
1058 level in a cell-specific manner and contributes to RNA immune evasion. *Nucleic*
1059 *Acids Res* **50**:9051–9071.
1060 Eijlers P, Al-Khafaji M, Soto-Martin E, Fasimoye R, Stead D, Wenzel M, Müller B, Pettitt J.
1061 2024. A nematode-specific ribonucleoprotein complex mediates interactions
1062 between the major nematode spliced leader snRNP and its target pre-mRNAs.
1063 *Nucleic Acids Res* **52**:7245–7260.
1064 Ellis RE. 2022. Sex Determination in Nematode Germ Cells. *Sex Dev* **16**:305–322.
1065 Ewels P, Magnusson M, Lundin S, Käller M. 2016. MultiQC: summarize analysis results
1066 for multiple tools and samples in a single report. *Bioinformatics* **32**:3047–3048.
1067 Fasimoye RY, Spencer REB, Soto-Martin E, Eijlers P, Elmassoudi H, Brivio S, Mangana C,
1068 Sabele V, Rechtorikova R, Wenzel M, Connolly B, Pettitt J, Müller B. 2022. A novel,
1069 essential *trans*-splicing protein connects the nematode SL1 snRNP to the CBC-
1070 ARS2 complex. *Nucleic Acids Res* **50**:7591–7607.

1071 Feder M, Pas J, Wyrwicz LS, Bujnicki JM. 2003. Molecular phylogenetics of the
1072 RrmJ/fibrillarin superfamily of ribose 2`-O-methyltransferases. *Gene* **302**:129–
1073 138.
1074 Furuichi Y, Morgan M, Shatkin AJ, Jelinek W, Salditt-Georgieff M, Darnell JE. 1975.
1075 Methylated, blocked 5 termini in HeLa cell mRNA. *Proc Natl Acad Sci U S A*
1076 **72**:1904–1908.
1077 Galloway A, Cowling VH. 2019. mRNA cap regulation in mammalian cell function and
1078 fate. *Biochimica et Biophysica Acta (BBA) - Gene Regulatory Mechanisms*
1079 **1862**:270–279.
1080 Garrison E, Marth G. 2012. Haplotype-based variant detection from short-read
1081 sequencing. *arXiv:12073907 [q-bioGN]*.
1082 Gene Ontology Consortium, Aleksander SA, Balhoff J, Carbon S, Cherry JM, Drabkin HJ,
1083 Ebert D, Feuermann M, Gaudet P, Harris NL, Hill DP, Lee R, Mi H, Moxon S,
1084 Mungall CJ, Muruganugan A, Mushayahama T, Sternberg PW, Thomas PD, Van
1085 Auken K, Ramsey J, Siegele DA, Chisholm RL, Fey P, Aspromonte MC, Nugnes
1086 MV, Quaglia F, Tosatto S, Giglio M, Nadendla S, Antonazzo G, Attrill H, Dos Santos
1087 G, Marygold S, Strelets V, Tabone CJ, Thurmond J, Zhou P, Ahmed SH,
1088 Asanitthong P, Luna Buitrago D, Erdol MN, Gage MC, Ali Kadhum M, Li KYC, Long
1089 M, Michalak A, Pesala A, Pritazahra A, Saverimuttu SCC, Su R, Thurlow KE,
1090 Lovering RC, Logie C, Oliferenko S, Blake J, Christie K, Corbani L, Dolan ME,
1091 Drabkin HJ, Hill DP, Ni L, Sitnikov D, Smith C, Cuzick A, Seager J, Cooper L, Elser
1092 J, Jaiswal P, Gupta P, Jaiswal P, Naithani S, Lera-Ramirez M, Rutherford K, Wood V,
1093 De Pons JL, Dwinell MR, Hayman GT, Kaldunski ML, Kwitek AE, Laulederkind SJF,
1094 Tutaj MA, Vedi M, Wang S-J, D'Eustachio P, Aimo L, Axelsen K, Bridge A, Hyka-

1095 Nouspikel N, Morgat A, Aleksander SA, Cherry JM, Engel SR, Karra K, Miyasato
1096 SR, Nash RS, Skrzypek MS, Weng S, Wong ED, Bakker E, Berardini TZ, Reiser L,
1097 Auchincloss A, Axelsen K, Argoud-Puy G, Blatter M-C, Boutet E, Breuza L, Bridge
1098 A, Casals-Casas C, Coudert E, Estreicher A, Livia Famiglietti M, Feuermann M,
1099 Gos A, Gruaz-Gumowski N, Hulo C, Hyka-Nouspikel N, Jungo F, Le Mercier P,
1100 Lieberherr D, Masson P, Morgat A, Pedruzzi I, Pourcel L, Poux S, Rivoire C,
1101 Sundaram S, Bateman A, Bowler-Barnett E, Bye-A-Jee H, Denny P, Ignatchenko A,
1102 Ishtiaq R, Lock A, Lussi Y, Magrane M, Martin MJ, Orchard S, Raposo P, Speretta
1103 E, Tyagi N, Warner K, Zaru R, Diehl AD, Lee R, Chan J, Diamantakis S, Raciti D,
1104 Zarowiecki M, Fisher M, James-Zorn C, Ponferrada V, Zorn A, Ramachandran S,
1105 Ruzicka L, Westerfield M. 2023. The Gene Ontology knowledgebase in 2023.
1106 *Genetics* **224**. doi:10.1093/genetics/iyad031
1107 Guo X, Zhang R, Wang J, Ding S-W, Lu R. 2013. Homologous RIG-I-like helicase proteins
1108 direct RNAi-mediated antiviral immunity in *C. elegans* by distinct mechanisms.
1109 *Proc Natl Acad Sci U S A* **110**:16085–16090.
1110 Haline-Vaz T, Silva TCL, Zanchin NIT. 2008. The human interferon-regulated ISG95
1111 protein interacts with RNA polymerase II and shows methyltransferase activity.
1112 *Biochem Biophys Res Commun* **372**:719–724.
1113 Haussmann IU, Wu Y, Nallasivan MP, Archer N, Bodi Z, Hebenstreit D, Waddell S, Fray R,
1114 Soller M. 2022. CMTr cap-adjacent 2`-O-ribose mRNA methyltransferases are
1115 required for reward learning and mRNA localization to synapses. *Nat Commun*
1116 **13**:1209.
1117 Hills-Muckey K, Martinez MAQ, Stec N, Hebbar S, Saldanha J, Medwig-Kinney TN, Moore
1118 FEQ, Ivanova M, Morao A, Ward JD, Moss EG, Ercan S, Zinovyeva AY, Matus DQ,

1119 Hammell CM. 2022. An engineered, orthogonal auxin analog/AtTIR1(F79G)
1120 pairing improves both specificity and efficacy of the auxin degradation system in
1121 *Caenorhabditis elegans*. *Genetics* **220**. doi:10.1093/genetics/iyab174
1122 Hyde JL, Diamond MS. 2015. Innate immune restriction and antagonism of viral RNA
1123 lacking 2`-O methylation. *Virology* **479–480**:66–74.
1124 Inesta-Vaquera F, Chaugule VK, Galloway A, Chandler L, Rojas-Fernandez A, Weidlich S,
1125 Peggie M, Cowling VH. 2018. DHX15 regulates CMTR1-dependent gene
1126 expression and cell proliferation. *Life Sci Alliance* **1**:e201800092.
1127 Jiao X, Chang JH, Kilic T, Tong L, Kiledjian M. 2013. A mammalian pre-mRNA 5` end
1128 capping quality control mechanism and an unexpected link of capping to pre-
1129 mRNA processing. *Mol Cell* **50**:104–115.
1130 Jiao X, Doamekpor SK, Bird JG, Nickels BE, Tong L, Hart RP, Kiledjian M. 2017. 5' End
1131 Nicotinamide Adenine Dinucleotide Cap in Human Cells Promotes RNA Decay
1132 through DXO-Mediated deNADding. *Cell* **168**:1015-1027.e10.
1133 Joseph BB, Blouin NA, Fay DS. 2017. Use of a Sibling Subtraction Method (SSM) for
1134 Identifying Causal Mutations in *C. elegans* by Whole-Genome Sequencing. *G3* .
1135 doi:10.1534/g3.117.300135
1136 Keith G. 1995. Mobilities of modified ribonucleotides on two-dimensional cellulose
1137 thin-layer chromatography. *Biochimie* **77**:142–144.
1138 Kelly WG, Xu S, Montgomery MK, Fire A. 1997. Distinct requirements for somatic and
1139 germline expression of a generally expressed *Caernorhabditis elegans* gene.
1140 *Genetics* **146**:227–238.

1141 Kesner JS, Chen Z, Shi P, Aparicio AO, Murphy MR, Guo Y, Trehan A, Lipponen JE,
1142 Recinos Y, Myeku N, Wu X. 2023. Noncoding translation mitigation. *Nature*
1143 **617**:395–402.
1144 Kiledjian M. 2018. Eukaryotic RNA 5`-End NAD+ Capping and DeNADding. *Trends Cell*
1145 *Biol* **28**:454–464.
1146 Kim D, Langmead B, Salzberg SL. 2015. HISAT: a fast spliced aligner with low memory
1147 requirements. *Nat Methods* **12**:357–360.
1148 Kimble J, Crittenden SL. 2007. Controls of germline stem cells, entry into meiosis, and
1149 the sperm/oocyte decision in *Caenorhabditis elegans*. *Annu Rev Cell Dev Biol*
1150 **23**:405–433.
1151 Krueger F. 2015. Trim Galore!: A wrapper around Cutadapt and FastQC to consistently
1152 apply adapter and quality trimming to FastQ files, with extra functionality for
1153 RRBS .... *Babraham Institute*.
1154 Kruse S, Zhong S, Bodi Z, Button J, Alcocer MJC, Hayes CJ, Fray R. 2011. A novel
1155 synthesis and detection method for cap-associated adenosine modifications in
1156 mouse mRNA. *Sci Rep* **1**:126.
1157 Kuge H, Brownlee GG, Gershon PD, Richter JD. 1998. Cap ribose methylation of c-mos
1158 mRNA stimulates translation and oocyte maturation in Xenopus laevis. *Nucleic*
1159 *Acids Res* **26**:3208–3214.
1160 Lasda EL, Kuersten S, Blumenthal T. 2011. SL *trans*-splicing in a *Caenorhabditis elegans*
1161 in vitro extract. *Cold Spring Harb Protoc* **2011**:db.prot5574.
1162 Lažetić V, Batachari LE, Russell AB, Troemel ER. 2023. Similarities in the induction of the
1163 intracellular pathogen response in *Caenorhabditis elegans* and the type I
1164 interferon response in mammals. *Bioessays* **45**:e2300097.

1165 Li H, Durbin R. 2010. Fast and accurate short read alignment with Burrows–Wheeler
1166 transform. *Bioinformatics* **25**:1754–1760.
1167 Li H, Handsaker B, Wysoker A, Fennell T, Ruan J, Homer N, Marth G, Abecasis G, Durbin
1168 R, 1000 Genome Project Data Processing Subgroup. 2009. The Sequence
1169 Alignment/Map format and SAMtools. *Bioinformatics* **25**:2078–2079.
1170 Li Y, Lu J, Han Y, Fan X, Ding S-W. 2013. RNA interference functions as an antiviral
1171 immunity mechanism in mammals. *Science* **342**:231–234.
1172 Liang S, Silva JC, Suska O, Lukoszek R, Almohammed R, Cowling VH. 2022. CMTR1 is
1173 recruited to transcription start sites and promotes ribosomal protein and histone
1174 gene expression in embryonic stem cells. *Nucleic Acids Res*.
1175 doi:10.1093/nar/gkac122
1176 Liao Y, Smyth GK, Shi W. 2014. featureCounts: an efficient general purpose program for
1177 assigning sequence reads to genomic features. *Bioinformatics* **30**:923–930.
1178 Love MI, Huber W, Anders S. 2014. Moderated estimation of fold change and dispersion
1179 for RNA-seq data with DESeq2. *Genome Biol* **15**:550.
1180 Mao K, Breen P, Ruvkun G. 2022. The *Caenorhabditis elegans* ARIP-4 DNA helicase
1181 couples mitochondrial surveillance to immune, detoxification, and antiviral
1182 pathways. *Proc Natl Acad Sci U S A* **119**:e2215966119.
1183 Mao K, Breen P, Ruvkun G. 2020. Mitochondrial dysfunction induces RNA interference in
1184 *C. elegans* through a pathway homologous to the mammalian RIG-I antiviral
1185 response. *PLoS Biol* **18**:e3000996.
1186 Meisel JD, Wiesenthal PP, Mootha VK, Ruvkun G. 2024. CMTR-1 RNA methyltransferase
1187 mutations activate widespread expression of a dopaminergic neuron-specific
1188 mitochondrial complex I gene. *Curr Biol*. doi:10.1016/j.cub.2024.04.079

1189 Mello CC, Kramer JM, Stinchcomb D, Ambros V. 1991. Efficient gene transfer in *C.*
1190 *elegans*: extrachromosomal maintenance and integration of transforming
1191 sequences. *EMBO J* **10**:3959–3970.
1192 Mount SM, Anderson P. 2000. Expanding the definition of informational suppression.
1193 *Trends Genet* **16**:157.
1194 Müller MBD, Kasturi P, Jayaraj GG, Hartl FU. 2023. Mechanisms of readthrough
1195 mitigation reveal principles of GCN1-mediated translational quality control. *Cell*
1196 **186**:3227-3244.e20.
1197 Nance J, Frøkjær-Jensen C. 2019. The *Caenorhabditis elegans* Transgenic Toolbox.
1198 *Genetics* **212**:959–990.
1199 Negishi T, Kitagawa S, Horii N, Tanaka Y, Haruta N, Sugimoto A, Sawa H, Hayashi K-I,
1200 Harata M, Kanemaki MT. 2022. The auxin-inducible degron 2 (AID2) system
1201 enables controlled protein knockdown during embryogenesis and development
1202 in *Caenorhabditis elegans*. *Genetics* **220**. doi:10.1093/genetics/iyab218
1203 Panek J, Gang SS, Reddy KC, Luallen RJ, Fulzele A, Bennett EJ, Troemel ER. 2020. A
1204 cullin-RING ubiquitin ligase promotes thermotolerance as part of the
1205 intracellular pathogen response in *Caenorhabditis elegans*. *Proc Natl Acad Sci U*
1206 *S A* **117**:7950–7960.
1207 Perez-Riverol Y, Bai J, Bandla C, García-Seisdedos D, Hewapathirana S, Kamatchinathan
1208 S, Kundu DJ, Prakash A, Frericks-Zipper A, Eisenacher M, Walzer M, Wang S,
1209 Brazma A, Vizcaíno JA. 2022. The PRIDE database resources in 2022: a hub for
1210 mass spectrometry-based proteomics evidences. *Nucleic Acids Res* **50**:D543–
1211 D552.

1212 Philippe L, Pandarakalam GC, Fasimoye R, Harrison N, Connolly B, Pettitt J, Müller B.
1213 2017. An *in vivo* genetic screen for genes involved in spliced leader *trans*-splicing
1214 indicates a crucial role for continuous *de novo* spliced leader RNP assembly.
1215 *Nucleic Acids Res* **45**:8474–8483.
1216 Picard-Jean F, Brand C, Tremblay-Létourneau M, Allaire A, Beaudoin MC, Boudreault S,
1217 Duval C, Rainville-Sirois J, Robert F, Pelletier J, Geiss BJ, Bisaillon M. 2018. 2`-O-
1218 methylation of the mRNA cap protects RNAs from decapping and degradation by
1219 DXO. *PLoS One* **13**:e0193804.
1220 Reddy KC, Dror T, Sowa JN, Panek J, Chen K, Lim ES, Wang D, Troemel ER. 2017. An
1221 intracellular pathogen response pathway promotes proteostasis in *C. elegans*.
1222 *Curr Biol* **27**:3544-3553.e5.
1223 Schindelin J, Arganda-Carreras I, Frise E, Kaynig V, Longair M, Pietzsch T, Preibisch S,
1224 Rueden C, Saalfeld S, Schmid B, Tinevez J-Y, White DJ, Hartenstein V, Eliceiri K,
1225 Tomancak P, Cardona A. 2012. Fiji: an open-source platform for biological-image
1226 analysis. *Nat Methods* **9**:676–682.
1227 Schmittgen TD, Livak KJ. 2008. Analyzing real-time PCR data by the comparative C(T)
1228 method. *Nat Protoc* **3**:1101–1108.
1229 Schuberth-Wagner C, Ludwig J, Bruder AK, Herzner A-M, Zillinger T, Goldeck M, Schmidt
1230 T, Schmid-Burgk JL, Kerber R, Wolter S, Stümpel J-P, Roth A, Bartok E, Drosten C,
1231 Coch C, Hornung V, Barchet W, Kümmerer BM, Hartmann G, Schlee M. 2015. A
1232 conserved histidine in the RNA sensor RIG-I controls immune tolerance to N1-
1233 2`-O-methylated self RNA. *Immunity* **43**:41–51.
1234 Senchuk MM, Dues DJ, Schaar CE, Johnson BK, Madaj ZB, Bowman MJ, Winn ME, Van
1235 Raamsdonk JM. 2018. Activation of DAF-16/FOXO by reactive oxygen species

1236 contributes to longevity in long-lived mitochondrial mutants in *Caenorhabditis*
1237 *elegans*. *PLoS Genet* **14**:e1007268.
1238 Shen Y, Zhang J, Calarco JA, Zhang Y. 2014. EOL-1, the homolog of the mammalian
1239 Dom3Z, regulates olfactory learning in *C. elegans*. *J Neurosci* **34**:13364–13370.
1240 Simabuco FM, Pavan ICB, Pestana NF, Carvalho PC, Basei FL, Campos Granato D, Paes
1241 Leme AF, Zanchin NIT. 2019. Interactome analysis of the human Cap-specific
1242 mRNA (nucleoside-2`-O-)-methyltransferase 1 (hMTr1) protein. *J Cell Biochem*
1243 **120**:5597–5611.
1244 Sowa JN, Jiang H, Somasundaram L, Tecle E, Xu G, Wang D, Troemel ER. 2020. The
1245 *Caenorhabditis elegans* RIG-I homolog DRH-1 mediates the intracellular
1246 pathogen response upon viral infection. *J Virol* **94**. doi:10.1128/jvi.01173-19
1247 Stiernagle T. 2006. Maintenance of *C. elegans*. *WormBook* 1–11.
1248 Tan X, Calderon-Villalobos LIA, Sharon M, Zheng C, Robinson CV, Estelle M, Zheng N.
1249 2007. Mechanism of auxin perception by the TIR1 ubiquitin ligase. *Nature*
1250 **446**:640–645.
1251 Tecle E, Chhan CB, Franklin L, Underwood RS, Hanna-Rose W, Troemel ER. 2021. The
1252 purine nucleoside phosphorylase *pnp-1* regulates epithelial cell resistance to
1253 infection in *C. elegans*. *PLoS Pathog* **17**:e1009350.
1254 The UniProt Consortium, Bateman A, Martin M-J, Orchard S, Magrane M, Ahmad S, Alpi
1255 E, Bowler-Barnett EH, Britto R, Bye-A-Jee H, Cukura A, Denny P, Dogan T,
1256 Ebenezer T, Fan J, Garmiri P, da Costa Gonzales LJ, Hatton-Ellis E, Hussein A,
1257 Ignatchenko A, Insana G, Ishtiaq R, Joshi V, Jyothi D, Kandasaamy S, Lock A,
1258 Luciani A, Lugaric M, Luo J, Lussi Y, MacDougall A, Madeira F, Mahmoudy M,
1259 Mishra A, Moulang K, Nightingale A, Pundir S, Qi G, Raj S, Raposo P, Rice DL,

1260 Saidi R, Santos R, Speretta E, Stephenson J, Totoo P, Turner E, Tyagi N, Vasudev P,
1261 Warner K, Watkins X, Zaru R, Zellner H, Bridge AJ, Aimo L, Argoud-Puy G,
1262 Auchincloss AH, Axelsen KB, Bansal P, Baratin D, Batista Neto TM, Blatter M-C,
1263 Bolleman JT, Boutet E, Breuza L, Gil BC, Casals-Casas C, Echioukh KC, Coudert
1264 E, Cuche B, de Castro E, Estreicher A, Famiglietti ML, Feuermann M, Gasteiger E,
1265 Gaudet P, Gehant S, Gerritsen V, Gos A, Gruaz N, Hulo C, Hyka-Nouspikel N,
1266 Jungo F, Kerhornou A, Le Mercier P, Lieberherr D, Masson P, Morgat A,
1267 Muthukrishnan V, Paesano S, Pedruzzi I, Pilbout S, Pourcel L, Poux S, Pozzato M,
1268 Pruess M, Redaschi N, Rivoire C, Sigrist CJA, Sonesson K, Sundaram S, Wu CH,
1269 Arighi CN, Arminski L, Chen C, Chen Y, Huang H, Laiho K, McGarvey P, Natale DA,
1270 Ross K, Vinayaka CR, Wang Q, Wang Y, Zhang J. 2023. UniProt: the Universal
1271 Protein Knowledgebase in 2023. *Nucleic Acids Res* **51**:D523–D531.
1272 Toczydlowska-Socha D, Zielinska MM, Kurkowska M, Astha N, Almeida CF, Stefaniak F,
1273 Purta E, Bujnicki JM. 2018. Human RNA cap1 methyltransferase CMTr1
1274 cooperates with RNA helicase DHX15 to modify RNAs with highly structured 5`
1275 termini. *Philos Trans R Soc Lond B Biol Sci* **373**:20180161.
1276 Tourasse NJ, Millet JRM, Dupuy D. 2017. Quantitative RNA-seq meta-analysis of
1277 alternative exon usage in *C. elegans*. *Genome Res* **27**:2120–2128.
1278 Wang VY-F, Jiao X, Kiledjian M, Tong L. 2015. Structural and biochemical studies of the
1279 distinct activity profiles of Rai1 enzymes. *Nucleic Acids Res* **43**:6596–6606.
1280 Werner M, Purta E, Kaminska KH, Cymerman IA, Campbell DA, Mittra B, Zamudio JR,
1281 Sturm NR, Jaworski J, Bujnicki JM. 2011. 2`-O-ribose methylation of cap2 in
1282 human: function and evolution in a horizontally mobile family. *Nucleic Acids Res*
1283 **39**:4756–4768.

Wickham H. 2016. Ggplot2: Elegant graphics for data analysis, 2nd ed, Use R! Cham, Switzerland: Springer International Publishing.

Yu G, Li F, Qin Y, Bo X, Wu Y, Wang S. 2010. GOSemSim: an R package for measuring semantic similarity among GO terms and gene products. *Bioinformatics* **26**:976–978.

Yu G, Wang L-G, Han Y, He Q-Y. 2012. clusterProfiler: an R package for comparing biological themes among gene clusters. *OMICS* **16**:284–287.

Yu YT, Shu MD, Steitz JA. 1998. Modifications of U2 snRNA are required for snRNP assembly and pre-mRNA splicing. *EMBO J* **17**:5783–5795.

Zhu A, Ibrahim JG, Love MI. 2019. Heavy-tailed prior distributions for sequence count data: removing the noise and preserving large differences. *Bioinformatics* **35**:2084–2092.

Züst R, Cervantes-Barragan L, Habjan M, Maier R, Neuman BW, Ziebuhr J, Szretter KJ, Baker SC, Barchet W, Diamond MS, Siddell SG, Ludewig B, Thiel V. 2011. Ribose 2`-O-methylation provides a molecular signature for the distinction of self and non-self mRNA dependent on the RNA sensor Mda5. *Nat Immunol* **12**:137–143.

1302 **SUPPLEMENTARY FIGURES**

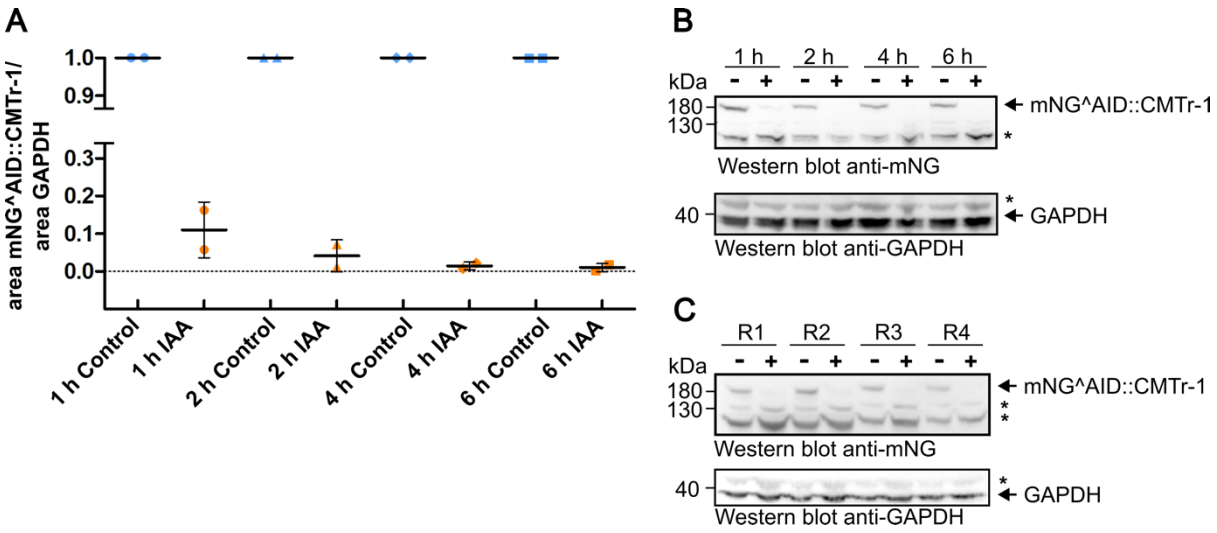

1303

1304 **Supplementary Figure 1. 5-Ph-IAA depletion of mNG^AID::CMTR-1.** (A) PE1176

1305 animals were treated with 5-Ph-IAA or control-treated and subjected to Western blotting at the

1306 indicated time points. Proteins were detected using anti-NeonGreen and anti-GAPDH

1307 antibodies. Protein levels of mNG^AID::CMTR-1 were standardised relative to GADPH, with the

1308 controls set to 1. Data represents 2 biological replicates. (B) Representative Western blot for the

1309 data shown in A. (C) Western blot of mNG^AID::CMTR-1 depletion of replicates (R1-4) used to

1310 generate RNA-Seq data (see Figure 6). In B and C, "+" indicates 5-Ph-IAA treated samples and "-

1311 " control samples, respectively.

1312

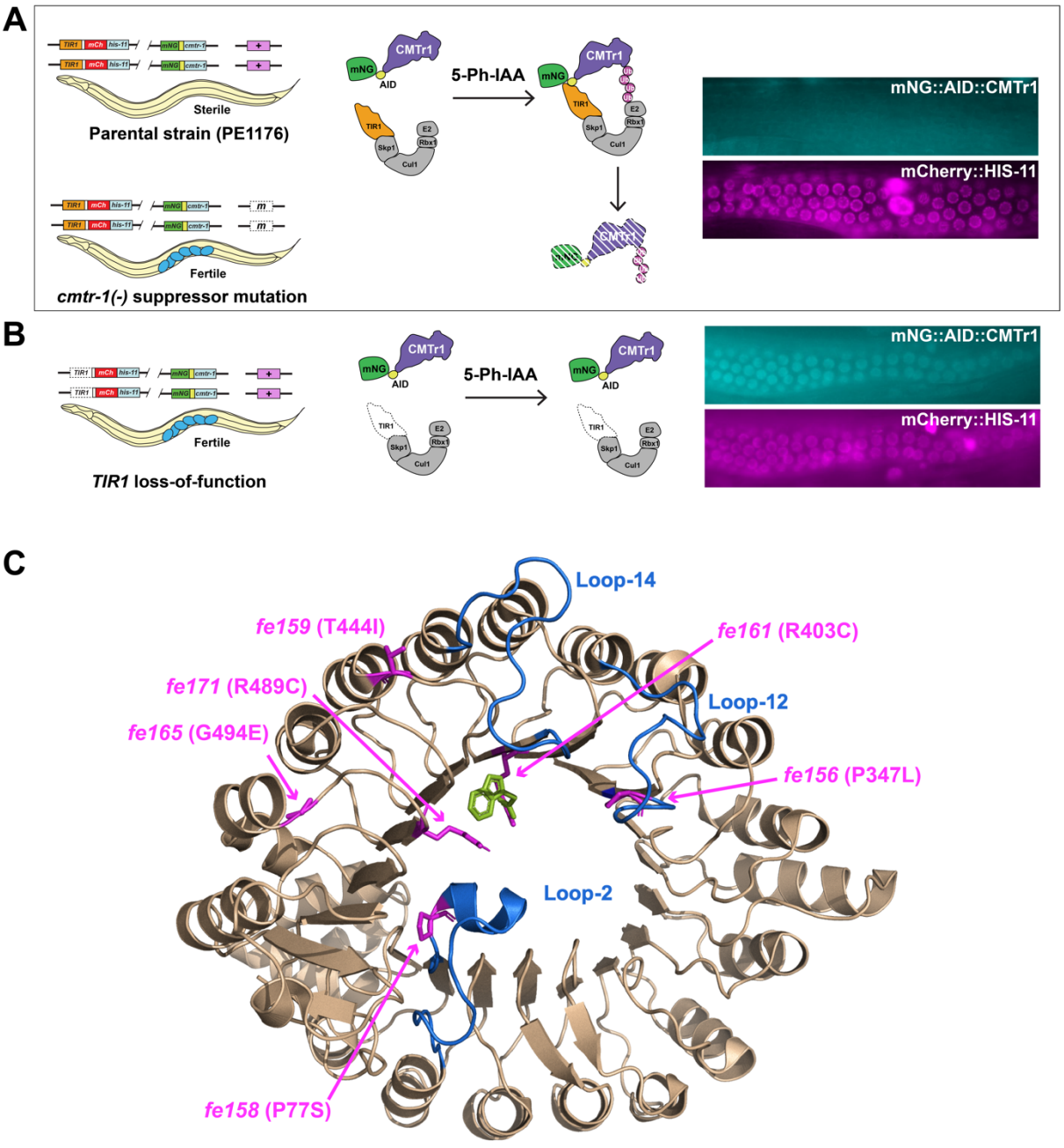

1313

1314 **Supplementary Figure 2. Secondary screen to distinguish suppressors epistatic to *cmtr-1(-)***
1315 **from *TIR1* loss-of-function mutants.** (A) The starting strain for the suppressor mutagenesis
1316 screen (PE1176) is sterile, while strains carrying suppressor mutations (m, unshaded, dashed
1317 box) that are epistatic to *cmtr-1(-)* restore fertility (blue ovals indicate eggs inside gravid
1318 hermaphrodites). (B) We predicted that TIR1 loss-of-function mutants (unshaded, dashed box)
1319 would also restore fertility to *cmtr-1(-)* animals, since these would prevent depletion of
1320 mNG^AID::CMTR-1. To distinguish between these two suppressor classes, we conducted a
1321 secondary screen based on mNeonGreen fluorescence. This was absent in PE1176 and
1322 epistatic suppressor strains (panels show distal gonad arms of adult hermaphrodites; nuclear

1323 mCherry::HIS-11 fluorescence was unaffected and serves to locate the germline nuclei), but
1324 was present in *TIR1* loss-of-function mutants. (C) Location of selected *TIR1* loss-of-function
1325 mutations identified from secondary screening (magenta). View of the TIR1-LRR domain
1326 showing the auxin and substrate-binding pocket (https://doi.org/10.2210/pdb2P1Q/pdb; (Tan et
1327 al., 2007)). Auxin is shown in green, the three extended loops key for the formation of the pocket
1328 are shown in blue.

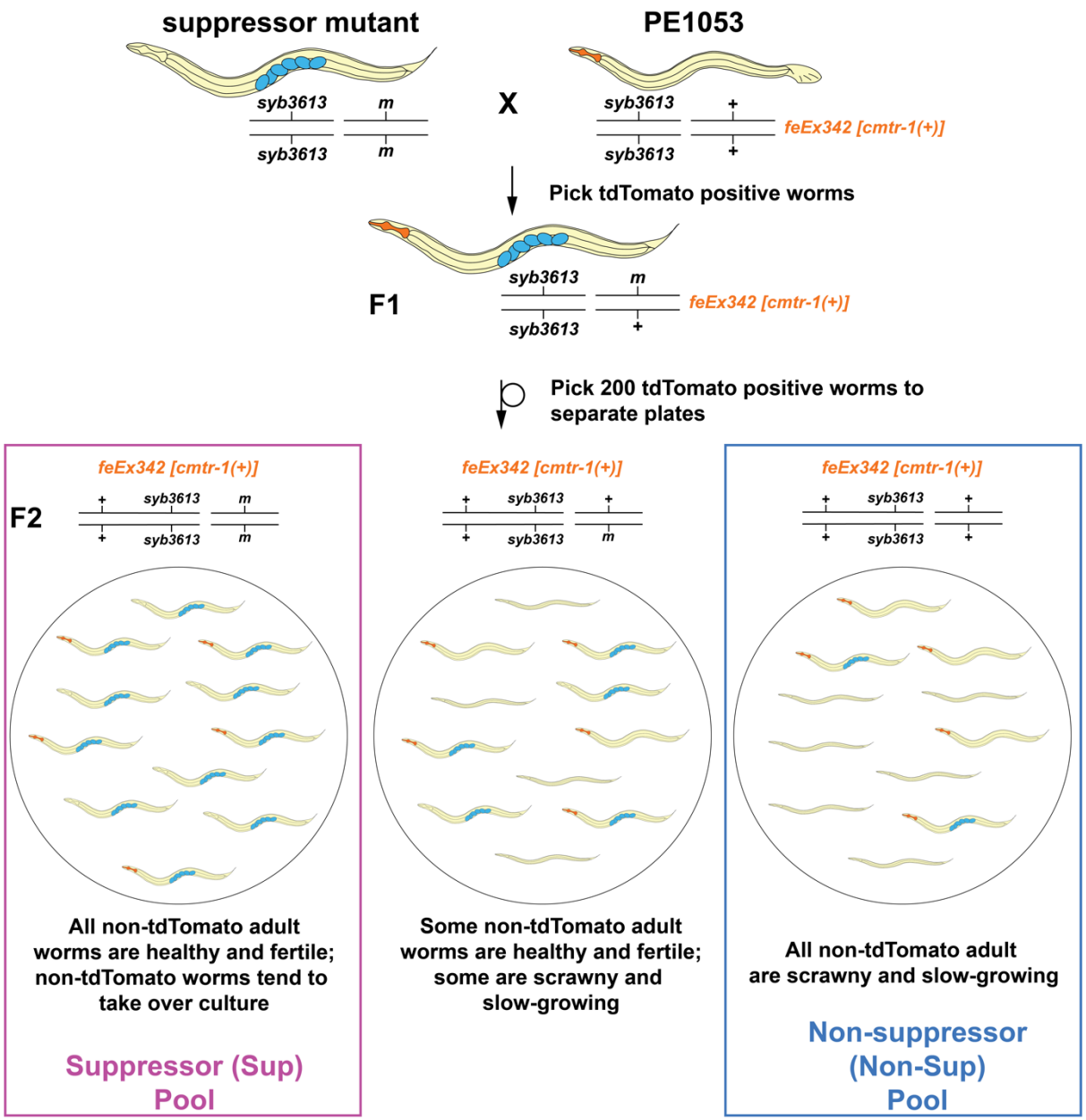

Figure 3. Strategy used to isolate strains for sibling-subtraction/whole genome sequencing mapping. Suppressor strains were crossed to the transgenic rescue line, PE1053, which is homozygous for *cmtr-1(syb3613)* but rescued by the *feEx342 cmtr-1(+)* transgene. The Sup and Non-Sup lines were established from single F2 animals on the basis that F2 suppressor homozygotes were not dependent on the *feEx342 cmtr-1(+)* transgene, while the broods of non-suppressor homozygotes resembled those of the PE1053 grandparent strain. Note, *feEx342* shows relatively poor rescue of the *cmtr-1* loss-of-function phenotype, so some transgenic animals are sterile. Transgenic animals were recognised on the basis of the *myo-2p::tdTomato* expression in the pharynx, which

1339 is also carried on the *feEx342* extrachromosomal transgenic array. Blue ovals indicate
1340 eggs inside gravid hermaphrodites.

SUPPLEMENTARY TABLES

Supplementary Table 1.

Strains and oligonucleotides.

Supplementary Table 2.

GFP::CMTR-1 and GFP::CMTR-2 immunoprecipitation data.

Supplementary Table 3.

PE1176 5-Ph-IAA treated versus control differential gene expression and GO enrichment analysis.

Supplementary Table 4.

Variant mapping for *fe152* and *fe154*. Only variants found in 100% of Sup reads, and absent in 100% of Non-Sup reads are shown. Highlights indicate variants found in both *fe152* and *fe154* Sup pools.